



## Sequestration of membrane cholesterol by cholesterol-binding proteins inhibits SARS-CoV-2 entry into Vero E6 cells

Magdalena Kulma<sup>a,§</sup>, Aleksandra Šakanović<sup>a,§,1</sup>, Apolonija Bedina-Zavec<sup>a</sup>, Simon Caserman<sup>a</sup>, Neža Omersa<sup>a</sup>, Gašper Šolinc<sup>a</sup>, Sara Orehek<sup>b</sup>, Iva Hafner-Bratkovič<sup>b,c</sup>, Urška Kuhar<sup>d</sup>, Brigita Slavec<sup>d</sup>, Uroš Krapež<sup>d</sup>, Matjaž Ocepek<sup>d</sup>, Toshihide Kobayashi<sup>e,f</sup>, Katarzyna Kwiatkowska<sup>g</sup>, Roman Jerala<sup>b,c</sup>, Marjetka Podobnik<sup>a</sup>, Gregor Anderluh<sup>a,\*</sup>

<sup>a</sup> Department of Molecular Biology and Nanobiotechnology, National Institute of Chemistry, Hajdrihova 19, 1000, Ljubljana, Slovenia

<sup>b</sup> Department of Synthetic Biology and Immunology, National Institute of Chemistry, Hajdrihova 19, 1000 Ljubljana, Slovenia

<sup>c</sup> EN-FIST Centre of Excellence, Trg Osvojitelne Fronte 13, 1000, Ljubljana, Slovenia

<sup>d</sup> Veterinary Faculty, University of Ljubljana, Gerbičeva 60, 1000, Ljubljana, Slovenia

<sup>e</sup> Lipid Biology Laboratory, RIKEN, 2-1, Hirosawa, Wako-shi, Saitama, 351-0198, Japan

<sup>f</sup> UMR 7021 CNRS, Université de Strasbourg, F-67401, Illkirch, France

<sup>g</sup> Laboratory of Molecular Membrane Biology, Nencki Institute of Experimental Biology of the Polish Academy of Sciences, 3 Pasteur St., 02-093, Warsaw, Poland

### ARTICLE INFO

#### Keywords:

Cholesterol  
Endocytosis  
Plasma membrane  
Membrane domains  
Pore-forming proteins  
SARS-CoV-2  
Viral infection

### ABSTRACT

Membrane lipids and proteins form dynamic domains crucial for physiological and pathophysiological processes, including viral infection. Many plasma membrane proteins, residing within membrane domains enriched with cholesterol (CHOL) and sphingomyelin (SM), serve as receptors for attachment and entry of viruses into the host cell. Among these, human coronaviruses, including severe acute respiratory syndrome coronavirus 2 (SARS-CoV-2), use proteins associated with membrane domains for initial binding and internalization. We hypothesized that the interaction of lipid-binding proteins with CHOL in plasma membrane could sequester lipids and thus affect the efficiency of virus entry into host cells, preventing the initial steps of viral infection. We have prepared CHOL-binding proteins with high affinities for lipids in the plasma membrane of mammalian cells. Binding of the perfringolysin O domain four (D4) and its variant D4<sup>E458L</sup> to membrane CHOL impaired the internalization of the receptor-binding domain of the SARS-CoV-2 spike protein and the pseudovirus complemented with the SARS-CoV-2 spike protein. SARS-CoV-2 replication in Vero E6 cells was also decreased. Overall, our results demonstrate that the integrity of CHOL-rich membrane domains and the accessibility of CHOL in the membrane play an essential role in SARS-CoV-2 cell entry.

### 1. Introduction

Membrane lipids and proteins form dynamic membrane domains capable of concentrating or segregating specific molecules. This organizational heterogeneity has functional and structural significance, as lateral membrane domains either hinder or facilitate interactions between membrane components, thereby controlling essential cellular functions, such as signal transduction [1], intracellular lipid and protein trafficking [2], spatial organization of the plasma membrane [3], endocytosis [4], and extracellular vesicle formation [5]. As cellular

lipids and lipid membrane domains play extensive roles in fundamental cellular processes, they are often placed in the spotlight, also because of their involvement in the complex interplay between pathogens and host cells.

Recent studies have provided new insights into the crucial role of membrane domains, enriched in tightly packed cholesterol (CHOL) and sphingolipids, in various steps of the life cycles of different viruses [6,7]. Membrane domains are sites with a high concentration of specific receptors involved in viral attachment and internalization as well as host immune and inflammatory responses [8–14]. Indeed, their disruption has been shown to inhibit the infectivity of the human

\* Corresponding author.

E-mail address: [gregor.anderluh@ki.si](mailto:gregor.anderluh@ki.si) (G. Anderluh).

<sup>1</sup> Present address: Institute of Cell Biology, Faculty of Medicine, University of Ljubljana, Vrazov trg 2, 1000 Ljubljana, Slovenia.

<sup>§</sup> Magdalena Kulma and Aleksandra Šakanović have contributed equally to the study.

### Abbreviations

<b>ACE2</b>	angiotensin-converting enzyme 2
<b>Alexa-RBD</b>	receptor-binding domain of the SARS CoV-2 spike protein labelled with Alexa-488
<b>ASM</b>	acid sphingomyelinase
<b>CDX</b>	methyl- $\beta$ -cyclodextrin
<b>CHOL</b>	cholesterol
<b>COVID-19</b>	coronavirus disease 2019
<b>D4</b>	domain four of the cholesterol-dependent cytolysin perfringolysin O
<b>DRM</b>	detergent-resistant membrane
<b>HRP</b>	horseradish peroxidase
<b>PEI</b>	polyethylenimine
<b>PFO</b>	perfringolysin O
<b>POPC</b>	1-palmitoyl-2-oleoyl- <i>sn</i> -glycero-3-phosphocholine
<b>RBD</b>	receptor-binding domain of the SARS CoV-2 spike protein
<b>RLU</b>	relative luciferase units
<b>SARS-CoV-2</b>	severe acute respiratory syndrome coronavirus 2
<b>SM</b>	sphingomyelin
<b>TMPRSS2</b>	transmembrane serine protease 2
<b>TX</b>	Triton X-100

immunodeficiency virus (HIV), human cytomegalovirus, influenza A, Ebola virus, Marburg virus, and the recently emerged pathogenic severe acute respiratory syndrome coronavirus 2 (SARS-CoV-2), the causative agent of the highly infectious coronavirus disease 2019 (COVID-19) [15–20]. In addition, the reduction of CHOL levels in the plasma membrane by apoA-I-binding protein, which stimulates cholesterol efflux, has been shown to have anti-HIV effects [21]. Moreover, alteration of cholesterol metabolism and trafficking influences the viral infection and propagation [22,23]. In this regard, studying the effect of the reduction of membrane domains by removing or sequestering the key membrane domains lipids represents a rapidly growing and attractive topic for antiviral research and the potential development of new and alternative therapeutic strategies [24,25].

SARS-CoV-2 is an enveloped, single-stranded, positive-sense RNA virus and belongs to the group of  $\beta$ -coronaviruses, that also includes the genetically closely related SARS-CoV-1 [26]. An important role in the initiation of infection of both viruses is played by the spike protein, which binds to the human angiotensin-converting enzyme type 2 (ACE2) receptor, facilitating virus entry into host cells [14, 27,28]. Another critical factor for both strains of SARS-related coronavirus infection is the cellular transmembrane serine protease 2 (TMPRSS2), which primes the spike protein allowing virus internalization [29,30]. Both the ACE2 receptor and TMPRSS2 have been shown to cluster in CHOL-rich domains [31,32]. Moreover, the process of virus internalization requires the presence of membrane CHOL, as CHOL depletion changes the spatial localization of the ACE2 receptor and reduces viral infectivity [13,19]. In addition, CHOL-rich membrane domains facilitate the fusion of SARS-CoV-2 with the host plasma membrane, thus promoting efficient virus entry [13,19].

Lipid components of the plasma membrane are also targets for the binding of pore-forming proteins, which are secreted by a variety of organisms from all kingdoms of life and used for attack or defense purposes in host-pathogen warfare [33]. Cholesterol-dependent cytolysins (CDCs) represent one of the best described pore-forming protein families, whose members are mainly secreted by pathogenic Gram-positive bacteria. CDCs are composed of four domains: D1 to D4. CHOL-specific binding to membranes is mediated by domain D4 [34]. D4 of the prototype member of this family, perfringolysin O (PFO), which is secreted by the pathogenic bacterium *Clostridium perfringens*, is

by itself non-toxic and has thus been used as a tool to visualize membrane CHOL after labelling with fluorescent proteins or dyes [35–41]. Furthermore, a mixture of CHOL and SM in the plasma membrane is essential for the interaction of the mushroom-derived non-toxic homologue of actinoporins, nakanori [16,42]. Previous studies suggested that nakanori can be used to study the organization and dynamics of SM/CHOL complexes and pre-existing SM/CHOL domains on the cell surface [16]. Additionally, binding of nakanori to epithelial cells has been shown to inhibit the release of influenza viruses from infected cells, suggesting the possibility of employing nakanori to disrupt the virus life cycle [16].

In this study, we analyzed the inhibitory effect of proteins that specifically recognize CHOL, a key lipid in the host plasma membrane, on virus entry into the cell. We showed that the CHOL-specific domain D4 of PFO and its variant D4<sup>E458L</sup> decreased the internalization of the receptor-binding domain (RBD) of the SARS-CoV-2 spike protein. Moreover, D4 and D4<sup>E458L</sup> exhibited an inhibitory effect on the entry of a pseudovirus complemented by the spike protein into cells and decreased cell infection with SARS-CoV-2 virus. Conversely, nakanori did not substantially decrease the cellular uptake of RBD or SARS-CoV-2-spike-bearing pseudoviruses or SARS-CoV-2 cell infection. Therefore, our results suggest that a specific pool of membrane CHOL must be sequestered by peripheral membrane proteins to prevent virus internalization. Altogether, the presented results open a new route for developing a potential molecular therapy for SARS-CoV-2 infection that is based on targeting membrane CHOL.

## 2. Material and methods

### 2.1. Materials

The plasmid vector pET28a-eGFP-nakanori was purchased from Riken (Japan). The plasmid vector coding for RBD was a kind gift from Prof. Dr. Ralf Wagner. The following was purchased: the gene coding for the D4<sup>E458L</sup> variant and amplification primers (Integrated DNA Technologies; USA); restriction enzymes (New England Biolabs; USA); T4 DNA ligase, DNase I, and Alexa-488® succinimidyl esters (Thermo Fisher Scientific; USA); lipids (Avanti Polar Lipids; Alabaster, USA); ACE2 (Sino Biological; 10108-H05H; China); and sensor chips and reagents for surface plasmon resonance (SPR) (Cytiva; Sweden). Other chemicals were from Sigma-Aldrich (USA), unless stated otherwise. The Vero E6, HeLa, HEK293T, and HEK293F cells were obtained from the American Type Culture Collection (ATCC).

### 2.2. Molecular cloning

To generate the expression vectors encoding CHOL-binding proteins, the corresponding gene fragments were subcloned into the pET28a or pET8c vectors with the N-terminal 6  $\times$  His tag. The restriction sites for subcloning were generated by PCR amplification using non-complementary ends of the amplification primers. The pET28a expression vector containing an eGFP-encoding sequence linked to the N-terminus of nakanori (Riken) was used as a template to prepare the vector encoding unlabelled nakanori (by removing the eGFP-encoding sequence using the restriction enzymes *NdeI/BamHI*) and the eGFP-fused D4 of PFO (residues 386–500). In the latter, the nakanori-coding sequence was replaced with the gene fragment encoding D4 using *EcoRI* and *BamHI*. The expression vector coding for the D4 variant D4<sup>E458L</sup>, which is genetically fused to domain three of the periplasmic protein TolA from *Escherichia coli* (residues 329–421), was prepared by subcloning the TolA-coding sequence from pTol with *XhoI* and *MluI* and subsequent 3'-insertion of the synthetic gene fragment. All constructs were verified by Sanger sequencing.

### 2.3. Protein expression and purification

All proteins except RBD were expressed in freshly transformed *E. coli* BL21(DE3) grown in LB medium supplemented with 30 µg/ml kanamycin (nakanori and D4 labelled N-terminally with eGFP) or 100 µg/ml ampicillin (D4, D4<sup>E458L</sup>) at 37 °C. Protein synthesis was induced with 0.5 mM isopropyl β-D-1-thiogalactopyranoside at the OD<sub>600</sub> of 0.6–0.8, and cells were grown for an additional 16–18 h at 20 °C. The bacterial biomass was harvested by centrifugation (15 min at 4000×g and 4 °C), resuspended to 10 ml/g wet mass in TBS buffer (20 mM Tris, 150 mM NaCl, pH 8.0) with added 10 mM imidazole, 50 µg/ml lysozyme, and 2 mM phenylmethylsulfonyl fluoride, incubated for 20 min at 4 °C, and lysed by sonication. Cell debris was removed by centrifugation (50 000×g for 1 h at 4 °C), and the supernatant was subjected to nickel-nitrilotriacetic acid (Ni-NTA) affinity purification on a 10 ml Ni-NTA column. Impurities were removed by washing with different imidazole concentrations (20, 50, and 100 mM) in TBS, pH 8.0. The proteins were eluted with 500 mM imidazole in TBS, dialyzed against 50 mM Tris-HCl, 150 mM NaCl, pH 7.5, or phosphate-buffered saline (PBS) and stored at –20 °C.

RBD of Spike protein (amino acids from 319 to 532) of the SARS-CoV-2 strain Wuhan-Hu-1 (NCBI YP\_009724390.1) was expressed with an N-terminal gp67 secretion signal peptide and a C-terminal 6 × His tag in HEK293-F cells, which were grown at 37 °C, 8 % CO<sub>2</sub> with 90 % relative humidity, and 120 rpm shaking in Expi293 Medium (Thermo Fisher Scientific, USA). Cells (3 × 10<sup>6</sup>/ml) were transformed with a plasmid coding for RBD using the ExpiFectamine™ 293 Transfection Kit (Thermo Fisher Scientific, USA). RBD secreted into cell medium was collected 72 h after transfection and purified as described previously [43]. Briefly, the medium containing the secreted protein was exchanged by HBS buffer (10 mM HEPES, 150 mM NaCl, pH 7.2). Next, the His-tagged RBD was captured on a 10 ml Ni-NTA column, washed with three column volumes of HBS with 50 mM imidazole, and eluted with 500 mM imidazole in HBS. The eluted fractions were further purified by size exclusion chromatography using Superdex 200 16/60 (GE Healthcare, USA) and HBS as a running buffer. Fractions containing pure protein were collected and concentrated (Merk Amicon MWCO 10 kDa, USA) to approximately 1 mg/ml, aliquoted, and stored at –80 °C until use.

### 2.4. Labelling of RBD with Alexa-488

The dye Alexa-488 was dissolved in DMSO to a final concentration of approximately 40 mg/ml, added to the purified protein up to 5 % (v/v), and incubated at 22–24 °C for 15 min. The non-conjugated dye was separated from labelled protein using spin filters. Protein concentration and the degree of labelling were measured as described previously [44]. The labelled protein was further concentrated to approximately 1 mg/ml and stored at –20 °C until use.

### 2.5. Protein-lipid overlay assay

To test the specificity of the proteins to isolated lipids, 1 µl of chloroform:methanol:water mixture (1:1:0.3, v:v:v) containing 1000 pmol of 1-palmitoyl-2-oleoyl-*sn*-glycero-3-phosphocholine (POPC), CHOL, and SM was applied to the PVDF membrane according to the procedure described previously [45]. The membrane was then treated with casein blocking buffer for 2 h and incubated overnight with 10 µg/ml recombinant proteins at 22–24 °C. Unbound proteins were removed by washing in TBS containing 0.03 % Tween-20. This was followed by incubation with mouse anti-His IgG (Qiagen, Germany) and then horseradish peroxidase (HRP)-coupled rabbit anti-mouse antibodies. Blots were developed by enhanced chemiluminescence substrate (Millipore, Billerica, USA), and chemiluminescence was captured with an iBright 15000 imaging system (Thermo Fisher Scientific, USA).

### 2.6. Vesicles preparation

The dissolved lipids were mixed in the desired molar ratios and vacuum-dried to form a lipid film. Multilamellar vesicles (MLVs) were prepared by hydrating the lipid film in PBS at 22–24 °C and vigorous vortexing, followed by six cycles of freezing and thawing in liquid nitrogen. The prepared MLVs were used for vesicle-sedimentation assays or to prepare large unilamellar vesicles (LUVs) for surface plasmon resonance (SPR) measurements by extruding them through a polycarbonate membrane with 100 nm diameter pores [46].

### 2.7. Vesicles-sedimentation assay

The sedimentation assay was carried out by incubating proteins (5 µM) with MLVs containing lipids (1 mM) for 45 min at 37 °C in a buffer composed of 10 mM Tris-HCl, 150 mM NaCl, pH 7.5. After incubation, samples were centrifuged for 15 min at 16 100×g and 22–24 °C. The supernatant was transferred to a new tube, whereas the pellet was washed with the buffer and centrifuged again. Both the pellet containing MLVs and bound proteins and the supernatant containing the unbound protein fraction were loaded onto SDS-PAGE, visualized using SimplyBlue SafeStain (Thermo Fisher Scientific, USA), analyzed using the iBright 15000 imaging system, and quantified densitometrically using GelQuant.NET software (BiochemLab Solutions, USA).

### 2.8. Surface plasmon resonance measurements

SPR experiments were performed using Biacore X100 (GE Healthcare, Sweden) and Biacore T200 (Cytiva, Sweden). Binding experiments were performed at 25 °C using 10 mM HEPES, pH 7.2, 150 mM NaCl, and 0.05 % P-20 surfactant as a running buffer for experiments with RBD (unlabelled and Alexa-RBD) and ACE2 (Sino Biological, China) or PBS with 0.5 % (w/v) bovine serum albumin for measuring the interaction of proteins and lipid vesicles.

ACE2 (25 µg/ml in Na acetate, pH 4.2) was immobilized on the CM5 sensor chip by the amine coupling method; the immobilization level was 300 RU. RBD titrations (9.4, 18.8, 37.5, 75, and 150 nM) were performed over immobilized ACE2 in a single-cycle mode with 90 s injections and 12 min final dissociation at a flow rate of 50 µl/min. Sensorgrams were double-referenced for evaluation. Experimental data were fitted to the 1:1 binding kinetic model (BiaEvaluation Software 3.2, GE Healthcare, Sweden) to obtain the kinetic parameters ( $k_a$  and  $k_d$ ) of the interaction and the  $K_D$ s. Experiments were performed in at least three technical replicates, and the results reported are the mean  $K_D$  ± standard deviation.

For studying interactions of the proteins and membranes, L1 sensor chips (Cytiva, Sweden) and LUVs with different lipid compositions were used. The chip surface was prepared as described previously [47,48]. A flow rate of 3 µl/min was used to load the vesicles. LUVs (100 or 200 µM) with different lipid compositions, namely POPC, POPC:SM (all lipid mixtures are at a 1:1 M ratio), POPC:CHOL, and SM:CHOL, were immobilized to the active flow cell, resulting in a response of approximately 1300 RU, while the reference flow cell was left empty. The other steps were performed at a flow rate of 30 µl/min. Nakanori, D4, or D4<sup>E458L</sup>, (all at 1 µM) were injected over the vesicles for 60 s, and dissociation was monitored for 4 min. The surface of the sensor chip was regenerated after each cycle with a 45 s injection of 40 mM *n*-octyl-β-D-glucopyranoside. Sensorgrams were double-referenced for final figures. Experiments were performed in at least three technical replicates, and a representative sensorgram is shown for each condition.

### 2.9. Fractionation of cell membranes

Vero E6 cells (CRL-1586, ATCC) (1.5 × 10<sup>6</sup>/sample) were pretreated with 10 mM methyl-β-cyclodextrin (CDX) or 100 mU/ml bacterial sphingomyelinase (SMase) for 1 h at 37 °C. Non-treated cells were used

as a control. After washing with PBS, cells were exposed to tested proteins (5  $\mu\text{M}$ ) for 45 min at 22–24 °C. Next, the cells were collected by centrifugation (4 min, 300 $\times$ g, 4 °C), washed in PBS, pH 7.4, and lysed with 70  $\mu\text{l}$  of 0.05 % Triton X-100 (TX) in buffer A (100 mM NaCl, 2 mM EDTA, 2 mM EGTA, 30 mM HEPES, pH 7.4, 1 mM phenylmethylsulfonyl fluoride) for 30 min at 4 °C. After centrifugation (5 min, 10 000 $\times$ g), the supernatant containing the Triton X-100-soluble (TX-soluble) fraction was collected, whereas the pellet was resuspended in 70  $\mu\text{l}$  of 1.8 % *n*-octyl- $\beta$ -D-glucopyranoside in buffer A and incubated for 30 min at 4 °C. After centrifugation, supernatant was collected as the detergent-resistant membrane (DRM) fraction, referring to its TX-insolubility. Equal volumes of DRM and TX-soluble fractions were loaded onto SDS-PAGE and subsequently transferred to nitrocellulose membranes for immunoblotting. The membranes were first blocked using casein blocking buffer, and then the binding of proteins to different fractions was detected with mouse anti-penta-HIS antibody (1:2000 dilution; Qiagen). Moreover, the antibodies goat anti-ACE2 (1:1000; R&D Systems), rabbit anti-flotillin-2 (1:2000; Cell Signaling Technology), and mouse anti- $\beta$ -actin (1:2000; Sigma-Aldrich) were used to detect the ACE2 receptor, flotillin, and  $\beta$ -actin, respectively. HRP-conjugated goat anti-mouse IgG (1:5000; Invitrogen), goat anti-rabbit IgG (1:5000; Merck Millipore), or rabbit anti-goat IgG (1:5000; Thermo Fisher Scientific) were used as secondary antibodies. The Amersham ECL Prime Western Blotting Detection Reagent and an iBright™ FL1500 imaging system were used for detection.

### 2.10. Toxicity assay

Protein toxicity was tested on Vero E6 and HEK293T (CRL-3216, ATCC) cells. One day before the experiment, Vero E6 cells were seeded onto a 96-well microtiter plate (at 35 000 cells/well) in culture medium (100  $\mu\text{l}$ /well). The next day, cells were rinsed twice with colorless Dulbecco's Modified Eagle Medium (DMEM) and incubated in dilutions of the tested proteins for 24 h. The dilutions of tested proteins were prepared in DMEM and used at a final concentration of up to 20  $\mu\text{M}$ . The next day, the viability of the treated cells was determined using PrestoBlue™ cell viability reagent (Thermo Fischer Scientific) according to the manufacturer's instructions. The relative viability of the treated cells was determined as a percentage of the viability of untreated cells. A similar toxicity assay was performed with HEK293T cells mimicking the cell density, protein concentrations, and incubation times of the pseudoviral assay (see below).

### 2.11. Confocal microscopy

Vero E6 cells and HeLa cells (CCL-2, ATCC) were cultured in Eagle's Minimum Essential Medium (EMEM) with 10 % fetal bovine serum (FBS) and maintained at 37 °C in an incubator with 5 % CO<sub>2</sub>. Vero E6 cells were seeded on chamber slides (Ibidi) and cultured for 2 days. Next, cells were rinsed twice with colorless DMEM medium and incubated for 2 h with a solution of lipid-binding proteins and/or fluorescent amine-modified polystyrene nanoparticles (Sigma-Aldrich L9904) or fluorescently labelled RBD at 37 °C. After incubation, cells were rinsed and observed either alive or after fixation with 4 % paraformaldehyde. In addition, cell suspensions from flow cytometry analysis were imaged to demonstrate nanoparticles and RBD protein uptake. Cell nuclei were stained with Hoechst 33342 (Thermo Fisher Scientific) at a final concentration of 20  $\mu\text{M}$ . Cells were imaged with a Leica TCS SP5 laser scanning microscope on a Leica DMI 6000 CS inverted microscope (Leica Microsystems, Germany) using a dry objective with 20 $\times$  magnification. Sequential excitation was performed with appropriate excitation lasers, and fluorescence emissions were recorded near the indicated emission peaks of each fluorophore, taking care not to overlap the signals (orange nanoparticles ex. 488 nm/em. 620–650 nm, Hoechst ex. 405 nm/em. 440–460 nm, eGFP ex. 488 nm/em. 515–520 nm, Alexa-488 labelled RBD ex. 488 nm/em. 510–560 nm, CellMask™ Deep Red Plasma

Membrane Stain (Invitrogen) ex. 633 nm/em. 660–700 nm).

Quantification of the fluorescence signal from polystyrene nanoparticles in Vero E6 cells was performed using Fiji software. A region of interest was drawn around each cell, and the area, integrated density, and mean fluorescence were measured. In addition, 4–8 adjacent background measurements were made. Values for integrated density were corrected for mean background fluorescence. For each treatment, 20–30 cells were quantified and analyzed using one-way ANOVA followed by Tukey's multiple comparisons test.

### 2.12. Flow cytometry

The uptake of RBD or fluorescently labelled, carboxyl-modified, red nanoparticle beads (100 nm in diameter) (Thermo Fisher Scientific) by Vero E6 or HeLa cells was assessed by flow cytometry. For this purpose, cells (300 000 cells/ml) were seeded onto 12-well plates and incubated overnight at 37 °C and 5 % CO<sub>2</sub>. The next day, medium was removed, and the cells were rinsed with DMEM. Subsequently, 100  $\mu\text{l}$  of DMEM and 100  $\mu\text{l}$  of a solution of the analyzed SM- and/or CHOL-binding proteins prepared in PBS or PBS as control were pre-incubated with cells for 15 min before Alexa-RBD (1  $\mu\text{M}$  final concentration) or red beads (10  $\mu\text{l}$ /well) were added. Samples were then incubated for 3 h at 37 °C. After incubation, the cells were washed with DMEM and detached from the surface with 0.05 % trypsin solution supplemented with 0.02 % EDTA. Cells were then pelleted by centrifugation (200 $\times$ g, 5 min), washed with medium containing 10 % FCS, and resuspended in 200  $\mu\text{l}$  of PBS. Additionally, to test the inhibitory effect of membrane lipid modulators, cells were incubated with CDX (5 mM final concentration) for 30 min or neutral SMase inhibitor GW4869 (5  $\mu\text{M}$  final concentration) for 2 h before incubation with the proteins. The cells containing fluorescently labelled RBD or red beads were detected using an Aurora spectral cytometer (Cytek) using excitation laser 488 nm and detectors B1 (498–518 nm) or B6 (606–630 nm). Results were analyzed using FlowJo software (BD Life Sciences) and expressed as median fluorescence intensity measured in three independent experiments.

### 2.13. VSV $\Delta$ G\* pseudoviral assay

A vesicular stomatitis virus-based pseudovirus system [49] was used to investigate the effect of the small lipid-binding protein domains on pseudovirus entry. The plasmids pCG1-hACE2, pCG1-SARS-2-S (encoding human codon-optimised sequence of Wuhan variant spike), and VSV $\Delta$ G\*/G virus were a kind gift from Stefan Pöhlmann (German Primate Center, Germany) [30]. Pseudoviruses, with genome-encoding GFP and Firefly luciferase that expressed upon infection, were prepared as described previously [30,50,51]. Briefly, HEK293T cells were plated at  $9 \times 10^5$  cells/well in a 6-well plate and after 24 h transfected with a pCG1-SARS-2-S plasmid using polyethylenimine (PEI) transfection reagent. The next day, cells were infected with VSV $\Delta$ G\*/G in a serum-free DMEM for 1 h at 37 °C. Afterward, the medium was removed, cells were washed with PBS and a complete medium containing an anti-VSV-G antibody (8G5F11, Kerastat, Boston, MA, USA) was added to the cells. Pseudovirus particles were harvested 18 h post inoculation, clarified from cellular debris by centrifugation (2000 $\times$ g, 10 min), aliquoted, and stored at –80 °C. For the pseudovirus assay, HEK293T cells were plated at  $2.5 \times 10^5$  cells/well onto a black 96-well plate with an optically clear bottom in 100  $\mu\text{l}$  of complete DMEM. The next day, they were transfected with Lipofectamine 2000 transfection reagent (Invitrogen) and plasmids encoding ACE2 (pCG1-ACE2), TMPRSS2 (pCMV3-C-Myc-TMPRSS2, Sinobiological), and Renilla luciferase (pRL-TK, Promega), the latter served to normalize Firefly luciferase luminescence. After 24 h, the transfected cells were pre-incubated with small lipid-binding protein domains for 10 min in serum-free DMEM before the pseudovirus was added. The next day, eGFP fluorescence (excitation 485 nm/emission 530 nm) was measured on the multiplate reader SynergyMx (BioTek), and cells were lysed in a passive lysis buffer

(Biotium). Luciferin substrate (Xenogen) was used to detect Firefly luciferase activity as a measure of pseudovirus infection, and coelenterazine H (Xenogen) was used to follow Renilla luciferase activity for determination of transfection efficiency on the luminometer Orion. Relative luminescence units (RLUs) were calculated by dividing values of Firefly luciferase with Renilla luciferase activity in each well.

#### 2.14. Antiviral assay

The antiviral activity of the selected proteins was tested on Vero E6 cells, maintained in EMEM (ATCC 30–2003) containing 10 % FBS (Gibco, Thermo Fisher Scientific, USA) and 1 % antibiotic and antimycotic (Gibco) at 37 °C in an incubator with 5 % CO<sub>2</sub>. All work with SARS-CoV-2 and cell cultures was performed in a biosafety level 3 laboratory. The patient-derived SARS-CoV-2 strain (Slovenia/SI-4265/20, D614G) was provided by the European Virus Archive (Ref# 005V-03961). The virus stock for further experiments was prepared on Vero E6 cells. Viral titer was determined by viral titration on Vero E6 cells and measured as 50 % tissue culture dose. Vero E6 cells were seeded ( $3.5 \times 10^4$  cells/well) onto a 96-well microtiter plate and incubated at 37 °C and 5 % CO<sub>2</sub>. The next day, cells were rinsed twice with DMEM and incubated with nakanori, D4 and D4<sup>E458L</sup>, diluted to final concentrations of 2.5, 5, 10, and 20 µM in DMEM or with DMEM only as a positive control. After a 5 min pre-incubation,  $100 \times 50$  % tissue culture dose of SARS-CoV-2 was added and incubated for 1 h. The virus-protein mixture was removed from the cells, and the cells were washed twice with DMEM. Fresh protein solutions in DMEM or DMEM only were added, and the cells were incubated for an additional 23 h. All incubation steps were performed in a cell culture incubator at 37 °C and 5 % CO<sub>2</sub>. DMEM added to the monolayer of washed Vero E6 cells and incubated for 24 h was used as a negative control. All treatments were performed in 5–8 technical replicates per experiment.

After 24 h of incubation, the culture medium was removed, and the cells were washed twice with DMEM. A synthetic trypsin TrypLE™ Express Enzyme (1X) in phenol red (Gibco) was used to detach the monolayers. The detached cells were used for RNA isolation using the MagMAX™ CORE Nucleic Acid Purification Kit on the KingFisher Flex System (Thermo Fisher Scientific). Viral RNA was measured with the real-time assay RT-qPCR targeting the E gene of SARS-CoV-2 using the primers and probe described by Corman et al. [52]. To detect endogenous controls, we used TaqMan Gene Expression Assays from Applied Biosystems (Thermo Fisher Scientific), the assay ID Hs99999901\_s1 (for 18S rRNA), and the assay ID Rh02621745-g1 (for GAPDH). For all RT-qPCR assays, AgPath-ID™ One-Step RT-qPCR Reagents (Thermo Fisher Scientific) were used. RT-qPCR was performed by QuantStudio 5 (Thermo Fisher Scientific) using 2 µl of the extracted total RNA. Thermal cycling for all assays was performed at 45 °C for 10 min for reverse transcription, followed by 95 °C for 10 min and then 45 cycles of 95 °C for 15 s and 58 °C for 45 s. Cycle threshold values (Ct) for viral E gene were determined in two subsequent measurements and presented as a mean value of the two. Ct values of reference genes 18S and GAPDH were averaged and used for normalization of the gene-of-interest Ct values, as in Riedel et al. [53].

#### 2.15. Statistical analysis

The results are shown as mean ± SD. Statistical analyses were performed by the GraphPad Prism version 8.4 or Origin 2018 software. Comparisons of parameters among three or more groups were made using one-way ANOVA for single-factor variables followed by Tukey's multiple comparisons test.

### 3. Results

#### 3.1. The selected lipid-binding proteins specifically recognize CHOL and/or SM

To explore the possibility of inhibiting SARS-CoV-2 infection by targeting membrane lipids of the host cell, we prepared a series of previously well-studied proteins that bind specifically to key lipids in mammalian membranes, such as CHOL and SM (Fig. 1a). We used the well-established membrane-binding domain (D4) of PFO as a CHOL-specific protein. Additionally, we had previously described a high-throughput approach for affinity selection of CHOL-specific D4 variants with substitutions at the membrane-interacting protein surface [54]. Among the most frequently selected variants, we identified the variant in which residue E458 is replaced by leucine (D4<sup>E458L</sup>), indicating high affinity and specificity for CHOL, thus making it a suitable candidate for testing inhibitory activity against SARS-CoV-2 infection. To increase the stability of D4<sup>E458L</sup> in solution, we genetically fused D4<sup>E458L</sup> to the third domain of the bacterial periplasmic protein TolA at the N-terminus [55], resulting in high yield, purity, and stability of the CHOL-specific protein. In parallel, we also tested the actinoporin-like protein nakanori that recognizes the SM/CHOL complex [16].

The purified recombinant CHOL-recognizing proteins were initially analyzed for their respective binding to both, the isolated lipids and the lipid vesicles with the desired lipid composition. The binding specificity for isolated lipids was analyzed with the protein-lipid overlay assay (Fig. 1b), whereas binding to lipid vesicles, namely MLVs and LUVs of different lipid compositions was investigated with the vesicle-sedimentation assay (Fig. 1c and d) and SPR (Fig. 1e), respectively. Nakanori is known as SM/CHOL-binding protein [16], however, the protein-lipid overlay assay showed the binding of nakanori mainly to CHOL and only in negligible quantities to SM (Fig. 1b), suggesting that recognition of CHOL is critical for interaction of nakanori with SM/CHOL complexes in membranes. In agreement with previous results [16], both SM and CHOL were needed for successful association of nakanori with lipid vesicles, in vesicle-sedimentation assay and SPR (Fig. 1c, d, e). The estimated amount of protein bound to MLVs composed of SM:CHOL was more than 70 % of the total protein nakanori bound to MLVs composed of SM:CHOL. By contrast, the fraction of the protein bound to MLVs containing only SM or CHOL did not exceed 10 % (Fig. 1d).

D4, as expected [56] bound specifically to CHOL and did not interact with SM or POPC in the protein-lipid overlay assay (Fig. 1b). Surprisingly, the vesicle-sedimentation assay revealed that D4 interacted not only with the CHOL-containing vesicles but also with vesicles composed of POPC:SM and POPC alone. SPR measurements showed the expected specific binding of D4 to immobilized vesicles composed of POPC:CHOL and not to vesicles composed of POPC, POPC:SM, or SM:CHOL. These data suggest that the short time of interaction (60 s) between LUVs and D4 in the SPR measurements demonstrate a higher affinity of D4 for binding with CHOL-containing vesicles while sedimentation assay observations suggest also less specific lipophilic interactions. The ambiguous character of D4 interactions in the sedimentation assay, prompted us to test a D4 derivative, in which the residue E458 is replaced by leucine (D4<sup>E458L</sup>) [54]. Similarly to D4, D4<sup>E458L</sup> specifically interacted with CHOL in the protein-lipid overlay assay (Fig. 1b) but, bound more selectively also to CHOL-containing vesicles (POPC:CHOL and SM:CHOL) in the sedimentation assay and SPR (Fig. 1c–e). Moreover, the obtained sensorgrams of D4<sup>E458L</sup> binding to SM:CHOL LUVs showed a slower dissociation rate compared to the binding to POPC:CHOL vesicles, indicating a more stable association with lipid bilayer containing CHOL in the presence of SM (Fig. 1e). The difference in affinity of D4 and D4<sup>E458L</sup> for CHOL-containing vesicles suggests that both proteins interact with different cholesterol pools or cholesterol organizations in the lipid bilayer. We can assume that the introduced E458L mutation favors the interaction with CHOL in the presence of SM versus POPC in

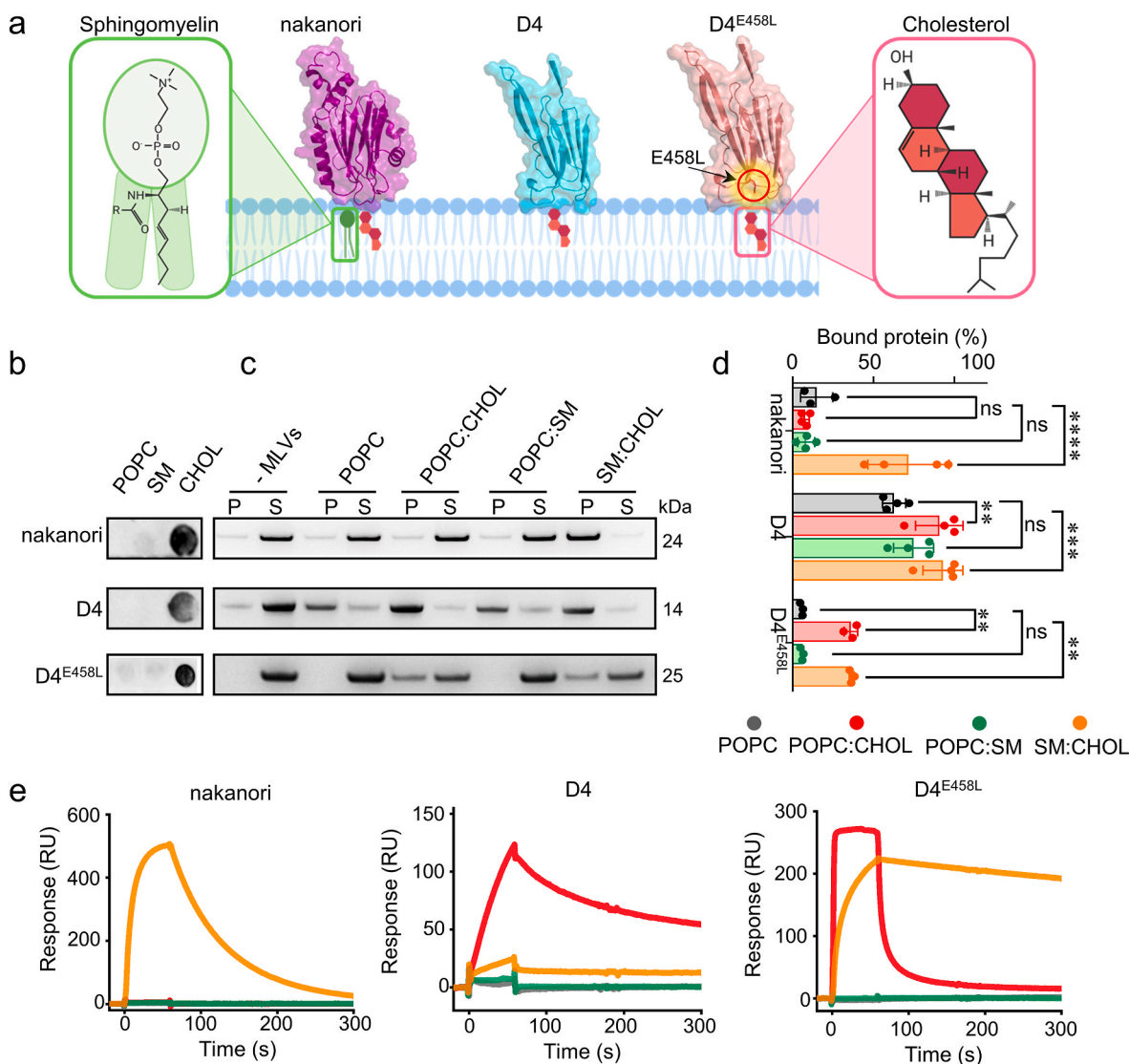


**Fig. 1. Lipid-binding specificity of the selected proteins.** (a) Schematic representation of the proteins used in this study and their lipid-binding specificity. (b) A representative protein-lipid overlay assay. 1 nmol of indicated lipids were spotted onto a nitrocellulose membrane and exposed to 10  $\mu\text{g}/\text{ml}$  lipid-binding proteins followed by anti-HIS IgG and anti-Mo IgG-HRP. Immunoreactive spots were detected by chemiluminescence. (c) A representative multilamellar vesicles (MLVs) sedimentation assay. MLVs composed of POPC, POPC/CHOL, POPC/SM and SM/CHOL (1 mM total lipids) were incubated with 5  $\mu\text{M}$  proteins. Bound proteins in the pellet (P) and unbound proteins remaining in the supernatant (S) were visualized on SDS-PAGE by SimplyBlue SafeStain staining. Experiments in b and c were performed in three or four independent repetitions. (d) Densitometric analysis of the amount of protein bound to MLVs detected in the pellet is expressed as percentage of total protein. Error bars depict standard deviations from three independent experiments. The standard deviation was determined from three independent repetitions. \*\* $p < 0.01$ , \*\*\* $p < 0.001$ , \*\*\*\* $p < 0.0001$ , ns represents no statistical difference ( $p > 0.05$ ). (e) Representative surface plasmon resonance sensorgrams of the binding of 1  $\mu\text{M}$  nakanori, D4, and D4 E458L to large unilamellar vesicles (LUVs) composed of POPC (gray), POPC:CHOL (red), POPC:SM (green), and SM:CHOL (orange), captured on the L1 sensor chip to a level of approximately 1300 RU. (For interpretation of the references to color in this figure legend, the reader is referred to the Web version of this article.)

the lipid bilayer.

Before assessing any possible inhibitory effects of the lipid-binding proteins on viral internalization processes, we analyzed their cytotoxicity on Vero E6 and HEK293T cells. No toxicity was observed with 10  $\mu\text{M}$  nakanori or 10  $\mu\text{M}$  D4 in Vero E6 and HEK293T cells. However, D4<sup>E458L</sup> only slightly reduced substrate conversion, for no more than 10 % at the highest, 10  $\mu\text{M}$  tested concentration for Vero E6 cells (Fig. 2a). Similar results were obtained with HEK293T cells (Fig. 2b).

### 3.2. The D4 localizes in the DRM fraction, whereas nakanori binds to the TX-soluble fraction of Vero E6 cell membranes

To determine whether nakanori and D4 utilize the same host membrane domains for binding, we performed Vero E6 cell partitioning,

which utilizes different detergent solubility of the membrane fractions. Namely, tightly packed SM and CHOL are defined by their insolubility in ice-cold Triton X-100 (TX) and solubility in *n*-octyl- $\beta$ -*D*-glucopyranoside [57]. After cell incubation with nakanori and D4, we used centrifugation to separate the fractions solubilized by TX and *n*-octyl- $\beta$ -*D*-glucopyranoside (DRM). In addition, we also analyzed the localization of the endogenously expressed ACE2 receptor and flotillin-2, a known protein marker for SM- and CHOL-enriched membrane domains, to confirm membrane partitioning. Moreover, we quantified the signal for cellular actin, which represents a measure for cell number, and used it to normalize the binding level of the analyzed lipid-binding proteins. The distribution of D4, nakanori, ACE2 receptor, and flotillin-2 between DRM and TX-soluble fractions was detected by immunoblotting (Fig. 3a and b). In accordance with previous studies, we

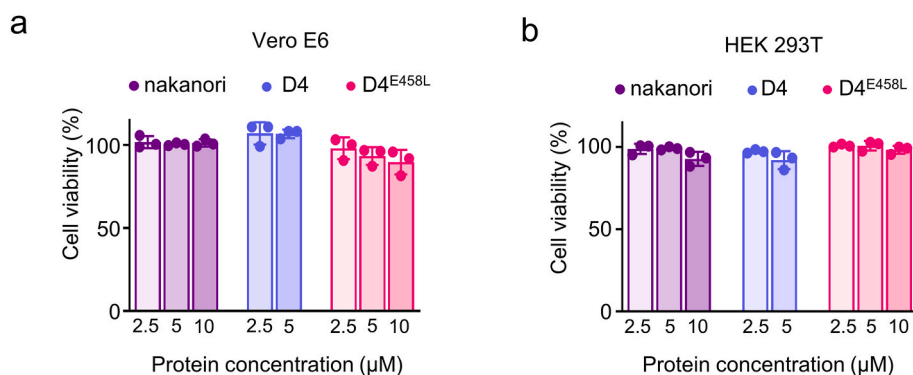


**Fig. 2.** Vero E6 cell and HEK293T viability after 24 h of incubation with proteins. (a) Vero E6 cells were incubated for 24 h in serum-free medium with nakanori (violet), D4 (cyan), D4<sup>E458L</sup> (red), at the indicated final concentrations to mimic the antiviral assay procedure. (b) In HEK293T cells, complete medium was added after a 10 min incubation with proteins in serum-free medium, thus mimicking the pseudoviral assay procedure. Viability is shown as substrate conversion level and expressed relatively to the untreated control. (For interpretation of the references to color in this figure legend, the reader is referred to the Web version of this article.)

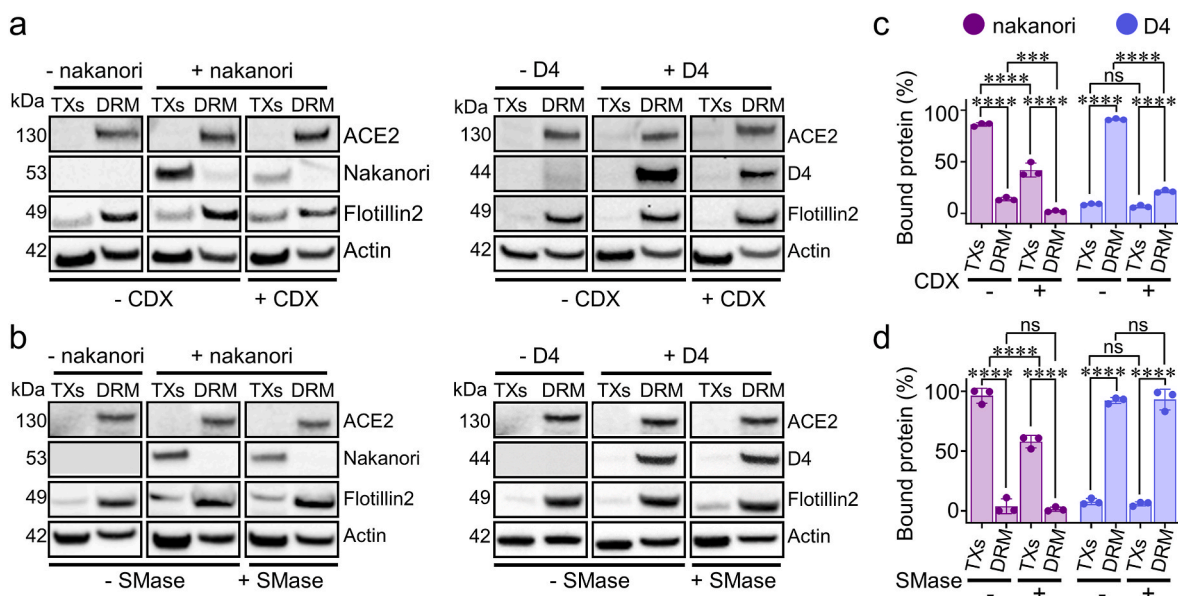


**Fig. 3.** D4 and nakanori show different distribution in membrane fractions upon binding to Vero E6 cells. (a), (b) Detection of the ACE2 receptor, flotillin-2, actin, and nakanori (left) or D4 (right) in the Triton X-100-soluble (TXs) and detergent-resistant membrane (DRM) fractions of Vero E6 cells. Vero E6 cells were pretreated with 10 mM methyl- $\beta$ -cyclodextrin (+CDX) (a) or 100 mU/ml SMase (+SMase) (b), or were left untreated (-CDX and -SMase, respectively) and subsequently incubated with 5  $\mu$ M eGFP-D4 or 5  $\mu$ M eGFP-nakanori. Next, the cell membranes were fractionated into the TXs and DRM fractions. Equal volumes of the fractions were subjected to SDS-PAGE, and the distribution of proteins was determined by immunoblotting. (c, d) Densitometry analysis of the amount of proteins bound to TXs or DRM fractions pretreated with CDX (c) or SMase (b). The amount of an individual protein in the membrane fractions was normalized to the total amount of actin in both fractions. Data are presented as mean  $\pm$  SEM of three independent experiments. \*\*\* $p$  < 0.001, \*\*\*\* $p$  < 0.0001, ns represents no statistical difference ( $p$  > 0.05).

showed colocalization of D4 and ACE2 with flotillin-2 in the DRM fraction [14, 31, 58]. Conversely, nakanori localized mainly in the TX-soluble fraction, where we detected approximately 80 % of the protein.

Additionally, we evaluated the effect of disrupting CHOL/SM domains on protein binding and localization. We disrupted membrane domains by CHOL extraction with CDX and hydrolysis of SM to ceramide by SMase. Prior to protein binding, Vero E6 cells were treated with CDX or SMase, and the distribution of D4, nakanori, ACE2, and flotillin-2 was determined by immunoblotting. The distribution of nakanori and D4 between TX-soluble and DRM fractions after treatment with CDX (Fig. 3a) and SMase (Fig. 3b) was quantified by densitometry (Fig. 3c and d). As expected, CHOL depletion reduced the binding level of both nakanori and D4. However, proteins were localized in the same fractions as before CDX treatment, namely, nakanori in the TX-soluble fraction

and D4 in the DRM fraction. Similarly, the localization of the ACE2 receptor was not influenced by membrane CHOL removal. Our results clearly show that both D4 and nakanori bind to the target membrane in a CHOL-dependent manner, but to different CHOL pools. In addition, we also verified the role of SM hydrolysis in the plasma membrane on D4 and nakanori binding to membrane fractions of Vero E6 cells. We observed that pretreating cells with SMase for 40 min significantly affected the binding of nakanori to cells (Fig. 3b). Binding to TX-soluble fractions was reduced nearly two-fold compared to untreated cells (Fig. 3b-d). As expected, SM hydrolysis exhibited no effect on the binding of D4 to Vero E6 membranes in the TX-soluble and DRM fractions (Fig. 3b-d). SMase treatment also did not affect ACE2 partition to the DRM fraction (Fig. 3b-d).

### 3.3. ACE2-dependent internalization of Alexa-RBD is reduced by D4 and D4<sup>E458L</sup> but not nakanori

The interaction between the RBD of the SARS-CoV-2 surface spike glycoprotein and the plasma membrane ACE2 receptor triggers a cascade of events leading to fusion between the cell and viral membranes, representing a critical first step for SARS-CoV-2 entry into target cells [28]. For this reason, we initially focused on determining the

potential inhibitory effect of SM- and/or CHOL-binding proteins on cellular internalization of Alexa-RBD due to sequestration of membrane lipids (Fig. 4a). We purified RBD, labelled it with fluorescent dye Alexa 488 and measured its binding affinity for the immobilized ACE2 receptor *in vitro* with SPR (Fig. 4b). Experimental data fitted to a 1:1 binding kinetic model showed that the binding of Alexa-RBD to the ACE2 receptor is in the nanomolar range, with a  $K_D$  of  $38.8 \pm 3.4$  nM ( $n = 5$ ). This affinity is 2–30-fold weaker than published results, which is

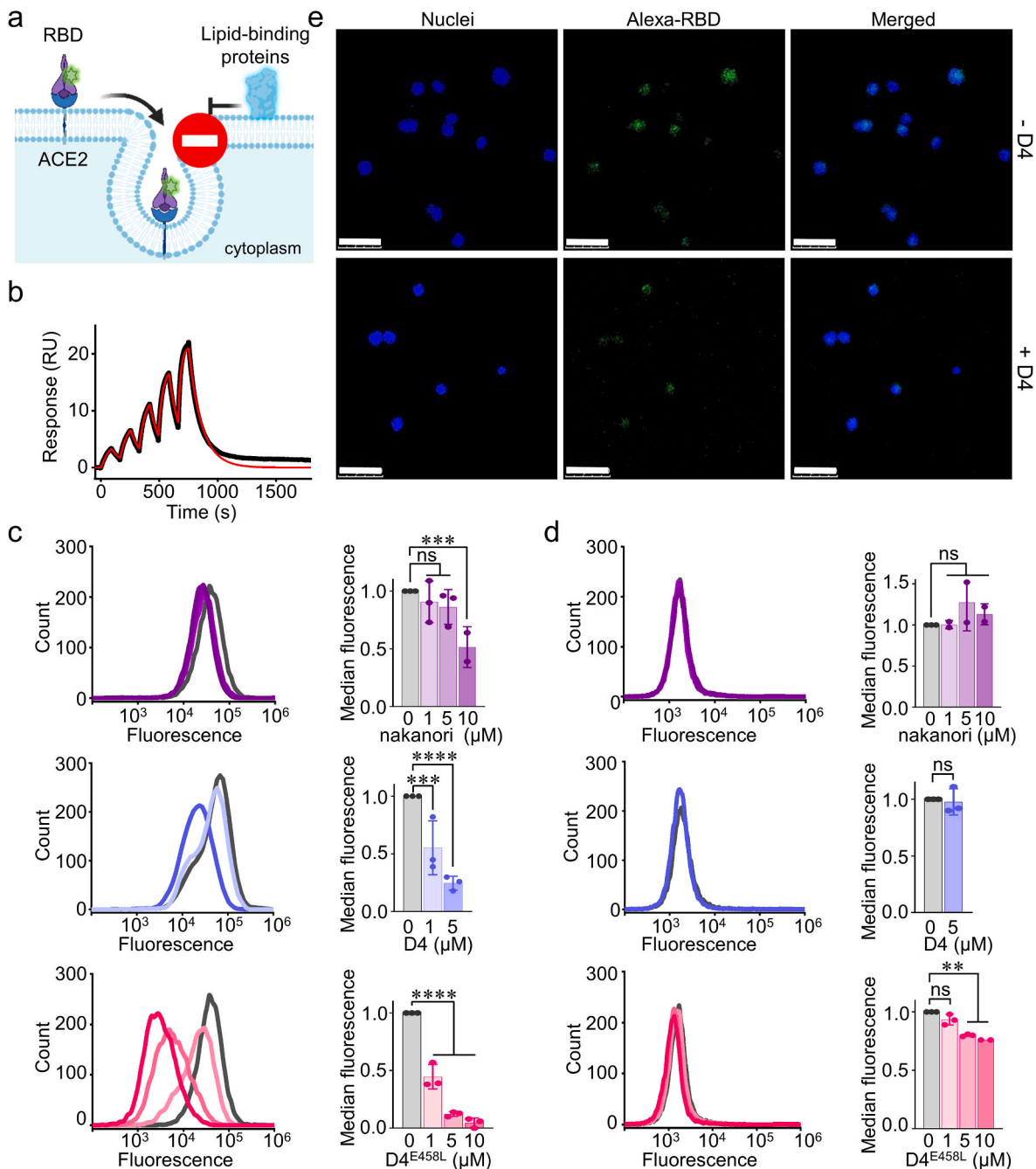


**Fig. 4.** D4 and D4<sup>E458L</sup>, but not nakanori, strongly reduce internalization of Alexa-receptor-binding domain (RBD) in Vero E6 cells. (a) Schematic representation of the sequestration of plasma membrane lipids by binding of peripheral lipid-binding proteins that inhibit cellular uptake of Alexa-RBD. (b) Representative sensorgram confirming binding of Alexa-RBD to immobilized ACE2 receptor. Five Alexa-RBD concentrations ranging from 9.4 nM to 150 nM in single-cycle mode were used. The black line shows the measured binding response and the red line the fit to the data according to a 1:1 binding model. (c) Vero E6 or (d) HeLa cells were incubated with the indicated concentrations of nakanori, D4 or D4<sup>E458L</sup> and 1 μM Alexa-RBD. Cell fluorescence was measured by flow cytometry and is shown by representative histograms (left) and relative median fluorescence intensity (mean ± SE) of two or three independent experiments (right). (e) Representative micrographs show Vero E6 cells incubated with fluorescently labelled RBD alone (upper panel) or together with 5 μM D4 (lower panel). Nucleus dye (Hoechst), blue; Alexa-RBD, green. Scale bar: 10 μm. \*\* $p < 0.01$ , \*\*\* $p < 0.001$ , \*\*\*\* $p < 0.0001$ , ns represents no statistical difference ( $p > 0.05$ ). (For interpretation of the references to color in this figure legend, the reader is referred to the Web version of this article.)

likely due to a different manufacturing process of the recombinant RBD protein [43,59–62].

To confirm that RBD internalization is ACE2-dependent, we used Vero E6 cells that endogenously express the ACE2 receptor and, as a control, HeLa cells that do not express the ACE2 receptor. We first exposed the cells to nakanori, D4, or D4<sup>E458L</sup> for 15 min and then added fluorescently labelled Alexa-RBD for 3 h. We observed a concentration-dependent lower fluorescence intensity of Vero E6 cells in the presence of D4 or D4<sup>E458L</sup>, indicating 75 % inhibition of Alexa-RBD

internalization at 5  $\mu$ M of D4 (Fig. 4c) and ca. 90 % at the same concentration of D4<sup>E458L</sup>, while no changes in fluorescence intensity of Alexa-RBD were observed in HeLa cells for D4 (Fig. 4d). Decreased cellular internalization of Alexa-RBD in D4-pre-treated compared to untreated Vero E6 cells was confirmed by confocal microscopy (Fig. 4e). Conversely, at the same concentration of nakanori inhibition of internalization of Alexa-RBD was not observed while 10  $\mu$ M only inhibited Alexa-RBD uptake by Vero E6 cells less significantly (Fig. 4c). It can be speculated that weak association of nakanori with CHOL-containing

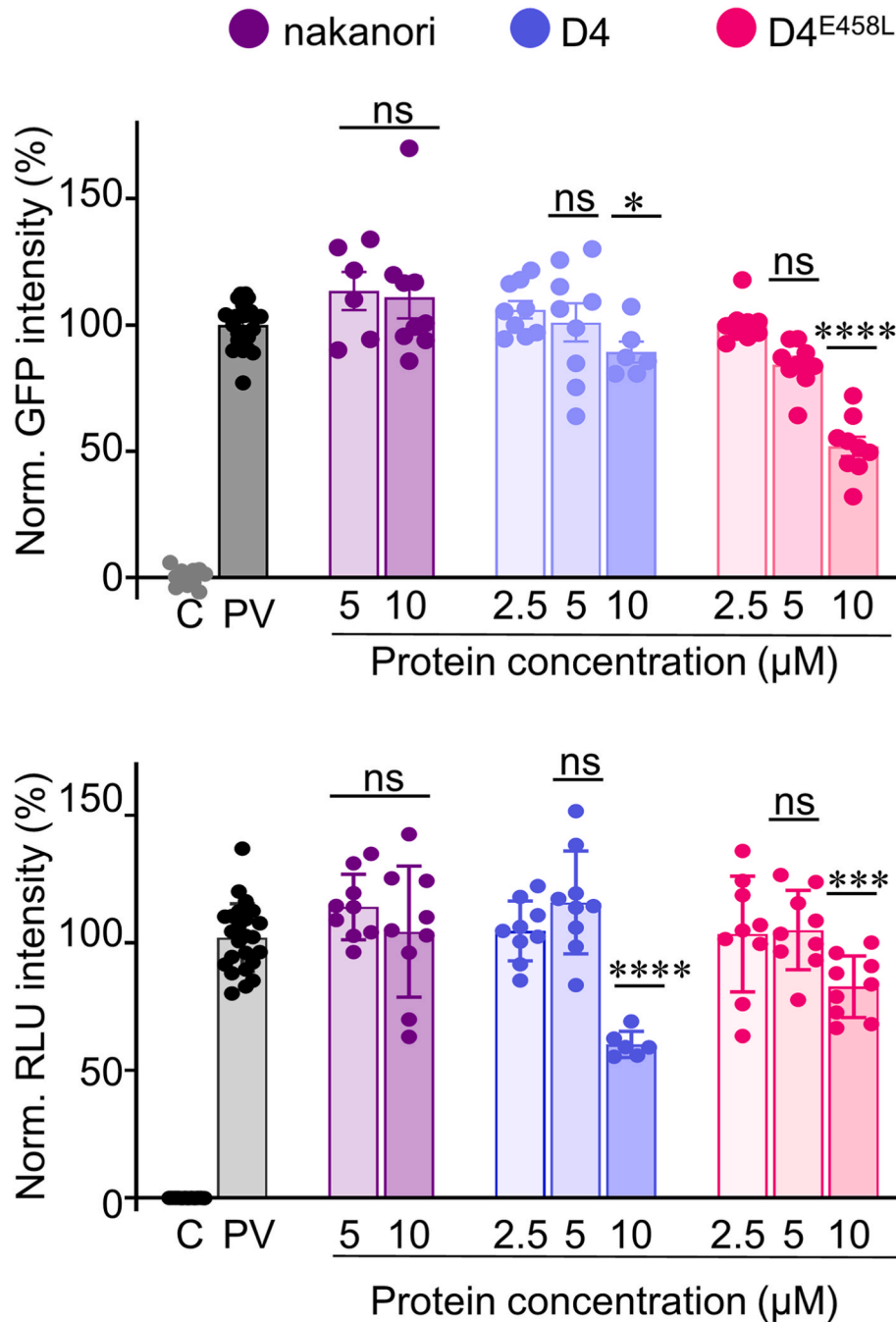


**Fig. 5.** D4 and D4<sup>E458L</sup> but not nakanori inhibit SARS-CoV-2 pseudovirus entry into ACE2-expressing HEK293T cells. ACE2-, TMPRSS2- and Renilla luciferase-expressing HEK293T cells were incubated with the indicated protein concentrations for 10 min prior to the addition of the pseudoviruses complemented with SARS-CoV-2 spike protein and encoding Firefly luciferase and eGFP. After 24 h, cells were lysed, and Firefly and Renilla luciferase activities or eGFP fluorescence were measured. The combined mean values of eGFP fluorescence (top) and relative luciferase units (RLU) (bottom) are normalized (Norm.) to the pseudovirus control (PV) without added lipid-binding proteins. Technical replicates from two or three independent experiments are shown as mean  $\pm$  SEM. Control (C) indicates cells not treated with pseudovirus. Comparison of statistical significances was done between the pseudovirus (PV) and the samples treated with 5 or 10  $\mu$ M proteins. \* $p$  < 0.05, \*\*\* $p$  < 0.001, \*\*\*\* $p$  < 0.0001, ns indicates no statistical difference ( $p$  > 0.05).

bilayer (Fig. 1e) may reflect reduced capacity of nakanori to prevent internalization of RBD. Therefore, inhibitory activity of nakanori on RBD uptake was observed at 10-fold higher concentration than D4. Compared with Vero E6 cells, the fluorescence intensity of Alexa-RBD in HeLa cells did not change significantly when the cells were incubated with the same concentrations of nakanori (Fig. 4d). Low inhibition of internalization of Alexa-RBD was found for 5 and 10  $\mu\text{M}$  D4<sup>E458L</sup> pre-treated HeLa cells, suggesting a small effect of the protein on the receptor-independent uptake of RBD (Fig. 4d). This confirmed that the changes in Vero E6 cell fluorescence were mainly due to inhibited ACE2-specific internalization of Alexa-RBD in the presence of the D4 or D4<sup>E458L</sup>.

### 3.4. D4 and D4<sup>E458L</sup>, but not nakanori, inhibit the entry of the pseudovirus carrying SARS-CoV-2 spike protein into ACE2-expressing HEK293T cells

The difference in the internalization level of RBD in Vero E6 cells in the presence of various cholesterol-binding proteins encouraged us to determine the effect of nakanori, D4, and D4<sup>E458L</sup> on pseudovirus entry into the cell. Hence, we used vesicular stomatitis pseudoviruses complemented with the SARS-CoV-2 spike protein to infect ACE2-expressing HEK293T cells. Firefly luciferase and GFP encoded in the pseudotyped virus served as markers of virus infection and allowed quantitative measurement of viral entry by detecting fluorescence and luminescence intensity (Fig. 5). To normalize transfection efficiency, we measured Renilla luciferase expression in the acceptor cells (not shown) and relative luciferase units were calculated by dividing Firefly luciferase units with Renilla luciferase units from respected well. After pre-incubation of cells with selected proteins (for 10 min), pseudoviral particles were added, and GFP fluorescence and Firefly and Renilla luciferase activities were measured 24 h after exposure (Fig. 5). Already 10  $\mu\text{M}$  concentrations of D4 and D4<sup>E458L</sup> reduced the pseudovirus entry of the ACE2- and TMPRSS2-expressing HEK293T cells. Conversely, under the same assay conditions, nakanori showed no effect on pseudovirus entry (Fig. 5).

### 3.5. D4 and D4<sup>E458L</sup> affect the amounts of viral RNA detected in Vero E6 cells after infection with SARS-CoV-2 virus

In the further step, we tested the ability of nakanori, D4, and D4<sup>E458L</sup> to inhibit SARS-CoV-2 virus infection of host cells. For this purpose, we pre-incubated Vero E6 cells with the proteins (at 2.5–20  $\mu\text{M}$ ) and then exposed them to a viral inoculum for 60 min. After the removal of the viral inoculum, cells were maintained in the presence of proteins due to possible reinfection cycles by a viral burst. After 24 h, intracellular viral RNA concentrations were quantified with RT-qPCR. Two reference genes were used to normalize the amount of viral RNA in host cells. In cells treated with D4 and D4<sup>E458L</sup> lower intracellular viral RNA was detected in a dose-dependent manner (Fig. 6). The highest differences in Ct values between controls and D4- or D4<sup>E458L</sup>-treated cells suggest a several hundred-fold decrease in viral RNA concentration. By contrast, detection of viral RNA in nakanori-treated cells exhibited variable levels depending on treatment with no clear effect compared to control.

### 3.6. Binding of D4 to the Vero E6 plasma membrane affects the internalization of fluorescent nanoparticles

The reduction in RBD internalization and pseudoviral endocytosis in the presence of D4 and D4<sup>E458L</sup> could be the result of ACE2 receptor shielding or a nonspecific effect on membrane lipids reorganization and consequent prevention of particles uptake. We speculate that in the latter case, binding of D4 might prevent other nonviral particles from entering the target cell. To gain further insights into the mechanisms of internalization inhibition by D4, we tracked cellular uptake of the fluorescent virus-sized spherical polystyrene fluorescent nano-beads. It has been shown that internalization of nanoparticles may be mediated by clathrin- and caveolin-dependent endocytosis [63], both cholesterol-dependent mechanisms that require specific plasma membrane lipid composition and organization [64]. To assess the potential impact of D4 on the cellular internalization process, we analyzed the binding and uptake of the nanoparticles in the presence of D4, which was genetically fused with eGFP that enabled the visualization of the D4 binding to cell membranes (eGFP-D4).

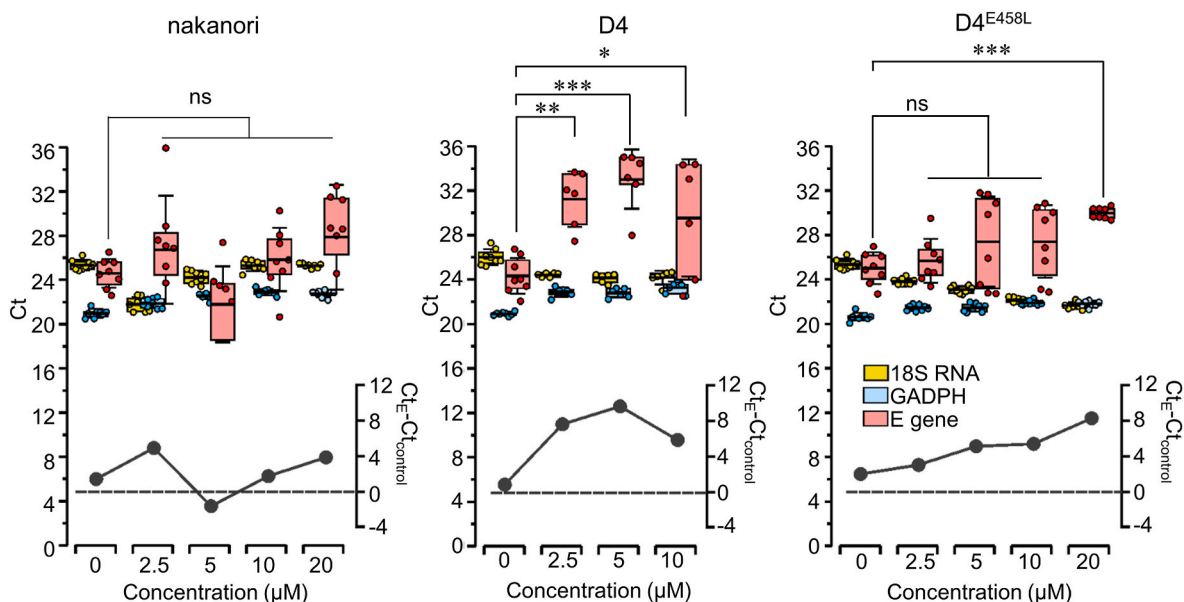


**Fig. 6.** D4 and D4<sup>E458L</sup> inhibit SARS-CoV-2 virus infection of Vero E6 cells. Ct values for the viral E gene and two reference genes, 18S RNA and GADPH, are shown for pre-incubation with different protein concentrations. Box plots represent Ct values of viral RNA amplification, showing mean Ct values  $\pm$  SD. The inset shows  $\Delta\text{Ct}$  values for E gene accounted for by the mean of both controls [53]. The untreated controls in nakanori and D4<sup>E458L</sup> are identical because the assay was performed on the same microplate. P values were calculated by ANOVA test for  $\Delta\text{Ct}$  values of treatment and control groups and show significant responses to D4 and D4<sup>E458L</sup> treatment. \* $p < 0.05$ , \*\* $p < 0.001$ , \*\*\* $p < 0.001$ , ns represents no statistical difference ( $p > 0.05$ ).

We used particles with negatively (carboxylated) and positively (aminated) charged surfaces. Vero E6 cells were incubated with nanoparticles upon treatment with eGFP-tagged D4 at concentrations of 0–10  $\mu$ M. The fluorescence intensity of the nanoparticles taken up by the cells was determined by flow cytometry (Fig. 7a). The analyzed cell suspension was examined by confocal microscopy, which showed that the particles were internalized into the cells (Fig. 7b). Both approaches revealed a decrease in fluorescence intensity of the particles in the cells that depended on eGFP-D4 concentration (Fig. 7c–e). Confocal microscopy revealed a predominant distribution of exogenously added eGFP-

tagged D4 on the cell surface (as could be expected in non-permeabilized cells [36, 56,66–67]) and a cytosolic distribution of nanoparticles (Fig. 7d). Presented results suggest that eGFP-D4, a CHOL-specific membrane binder, affects the cellular processes required for internalization of nanoparticles. Similar results were obtained regardless of nanoparticle surface charge as indicated in description to Fig. 7.

It is known that SARS-CoV-2 infection depends on SM/CHOL-rich membrane domains and that CDX inhibits the entry of SARS-CoV spike protein-bearing pseudoviruses in a dose-dependent manner in Vero E6 cells [68]. Strong inhibition of RBD uptake by Vero E6 cells in

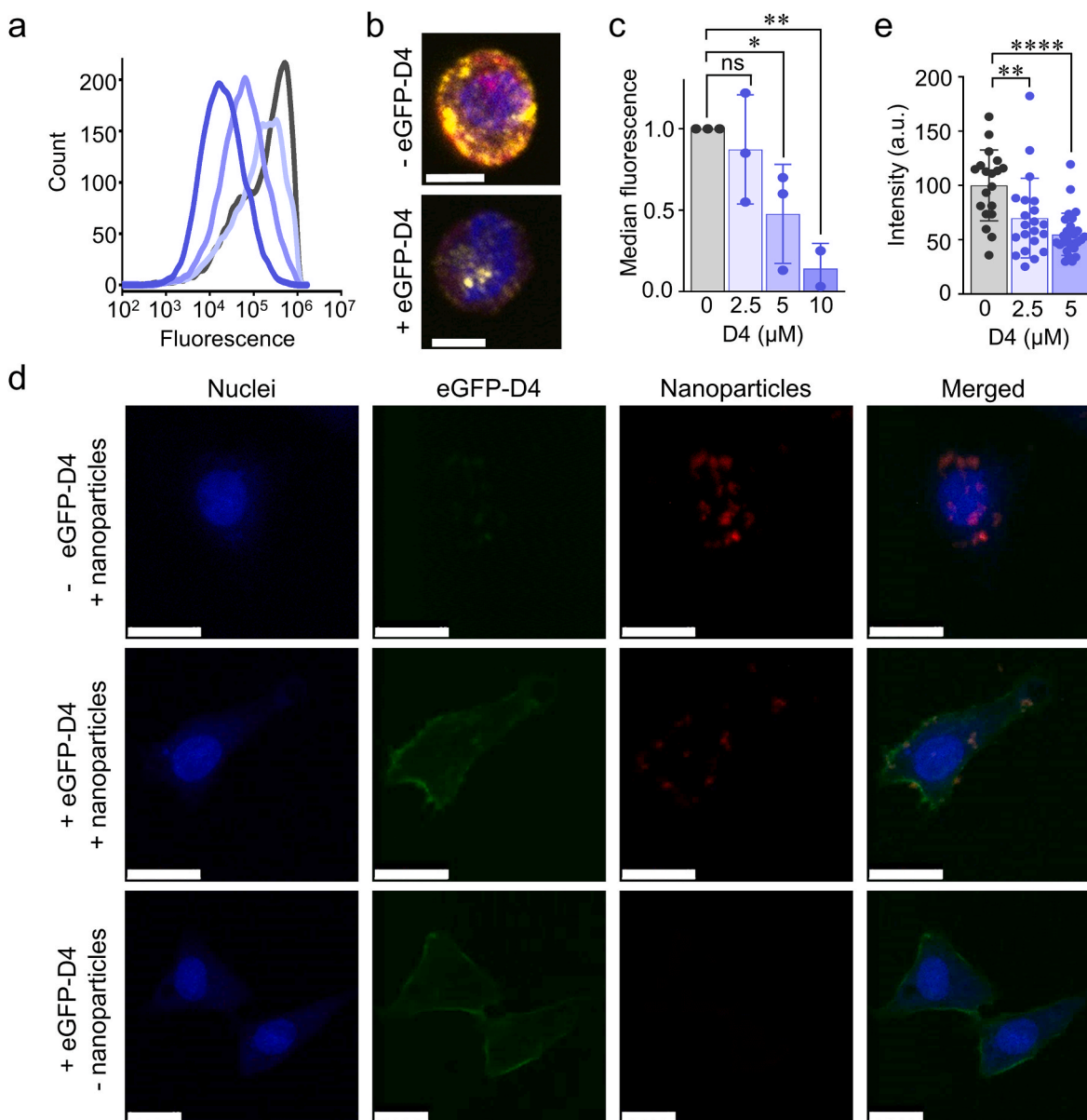


**Fig. 7. eGFP-tagged D4 reduces uptake of fluorescent nanoparticles by Vero E6 cells.** (a) The representative distribution of fluorescence intensity of cells. Vero E6 cells were preincubated with eGFP-tagged D4 (2.5  $\mu$ M (light blue), 5  $\mu$ M (blue), or 10  $\mu$ M (dark blue)); black line shows the data for non-treated Vero E6 cells) for 15 min before negatively charged nanoparticles were added. (b) The perinuclear confocal plane of the Vero E6 cells used in flow cytometry analysis (a) stained with CellMask plasma membrane stain, fixed and imaged under a confocal microscope. In the -eGFP-D4 cells, fluorescently labelled nanoparticles are distributed in the perinuclear region but not on the cell surface. The concentration of D4 was 5  $\mu$ M. Plasma membrane, red; nucleus, blue; nanoparticles, yellow. Scale bar: 10  $\mu$ m. (c) The relative median fluorescence intensity (mean  $\pm$  SE) of three independent experiments from the data presented in (a). (d) Representative fluorescence micrographs showing the uptake of positively charged polystyrene nanoparticles (red fluorescence) by Vero E6 cells in the presence of eGFP-D4 (5  $\mu$ M; + eGFP-D4), no eGFP-D4 (-eGFP-D4), or eGFP-D4 (5  $\mu$ M) only (+eGFP-D4, - nanoparticles) are shown in separate fluorescence channels and merged images. Cells were pretreated with or without 5  $\mu$ M eGFP-D4, and then nanoparticles (red) were added for 2 h at 37  $^{\circ}$ C. After incubation and fixation cell nuclei were stained with Hoechst (blue) and cells were imaged after sequential excitation with appropriate laser. Scale bars: 25  $\mu$ m. (e) Integrated signal density generated by red nanoparticles from Vero E6 cells pretreated with 2.5  $\mu$ M or 5  $\mu$ M eGFP-D4, assessed by image analysis, performed using Fiji. \* $p$  < 0.05, \*\* $p$  < 0.01, \*\*\*\* $p$  < 0.0001, ns represents no statistical difference ( $p$  > 0.05). (For interpretation of the references to color in this figure legend, the reader is referred to the Web version of this article.)

the presence of D4<sup>E458L</sup> prompted us to verify whether the inhibition of Alexa-RBD internalization is a CHOL-dependent process. We showed that preincubation of cells with CDX, hence CHOL depletion, inhibited Alexa-RBD entry into Vero E6 cells and attenuated the D4<sup>E458L</sup>-induced inhibition of Alexa-RBD entry (Fig. 8a). This result indicates that the inhibitory effect of D4<sup>E458L</sup> on Alexa-RBD internalization is CHOL-dependent. It is also known that the interaction of SARS-CoV-2 with ACE2 activates acid sphingomyelinase in cells and induces the accumulation of highly lipophilic, gel-like ceramide-rich domains at the cell surface [69]. Inhibition of acid sphingomyelinase prevents cellular infection with SARS-CoV-2, and indeed, some clinically approved drugs used to treat COVID-19 inhibit the function of acid sphingomyelinase [6, 68]. Neutral sphingomyelinase is also responsible for ceramide production, however its impact on SARS-CoV2 infection has not been fully understood [70]. We aimed to assess contribution of neutral sphingomyelinase to the uptake of RBD. To this end, the neutral sphingomyelinase-2 inhibitor GW4869 alone or in combination with D4<sup>E458L</sup> was used. GW4869 inhibited Alexa-RBD entry, and the combination of GW4869 and D4<sup>E458L</sup> potentially reduced Alexa-RBD entry into Vero E6 cells (Fig. 8b).

#### 4. Discussion

Most research on the SARS-CoV-2 virus has focused on proteins that play a critical role in the initial attack and entry of the virus into the host

cell; namely the spike protein and its interaction with ACE2 receptors [27,28]. However, the lipid components of the plasma membrane are also critical for the internalization and release of various viruses. Therefore, strategies that utilize host membrane lipids as molecular targets for antiviral activities have become increasingly studied [25, 71–73]. Several findings indicate that CHOL in the mammalian plasma membrane is essential for many viral infections, including SARS-CoV-2 infection [18,19,24,31].

CHOL is a major lipid in the plasma membrane of mammalian cells, and three pools of CHOL with different distributions in the plasma membrane were recently proposed to exist: (i) a CHOL pool that is accessible to CHOL-binding proteins, (ii) an SM-sequestered CHOL pool that becomes accessible after treatment with SMase, and iii) an essential CHOL pool that cannot be released by SMase [74]. The CDC family members PFO and anthrolysin O (especially, their D4 domain) bind to the accessible pool of CHOL [75]. Binding of anthrolysin O D4 sequesters accessible CHOL in the plasma membrane and thereby blocks the otherwise rapid transport of CHOL to the endoplasmic reticulum. Additionally, ostreolysin, a pore-forming protein from the aegerolysin family, binds to SM-CHOL complexes and specifically recognizes the SM-sequestered pool of CHOL, drastically altering intracellular CHOL trafficking [76]. Based on these findings, it has been suggested that SM/CHOL complexes may be enriched in areas of the plasma membrane where endocytosis occurs and that the accessible CHOL is excluded from these areas. Despite the growing number of studies showing the role of

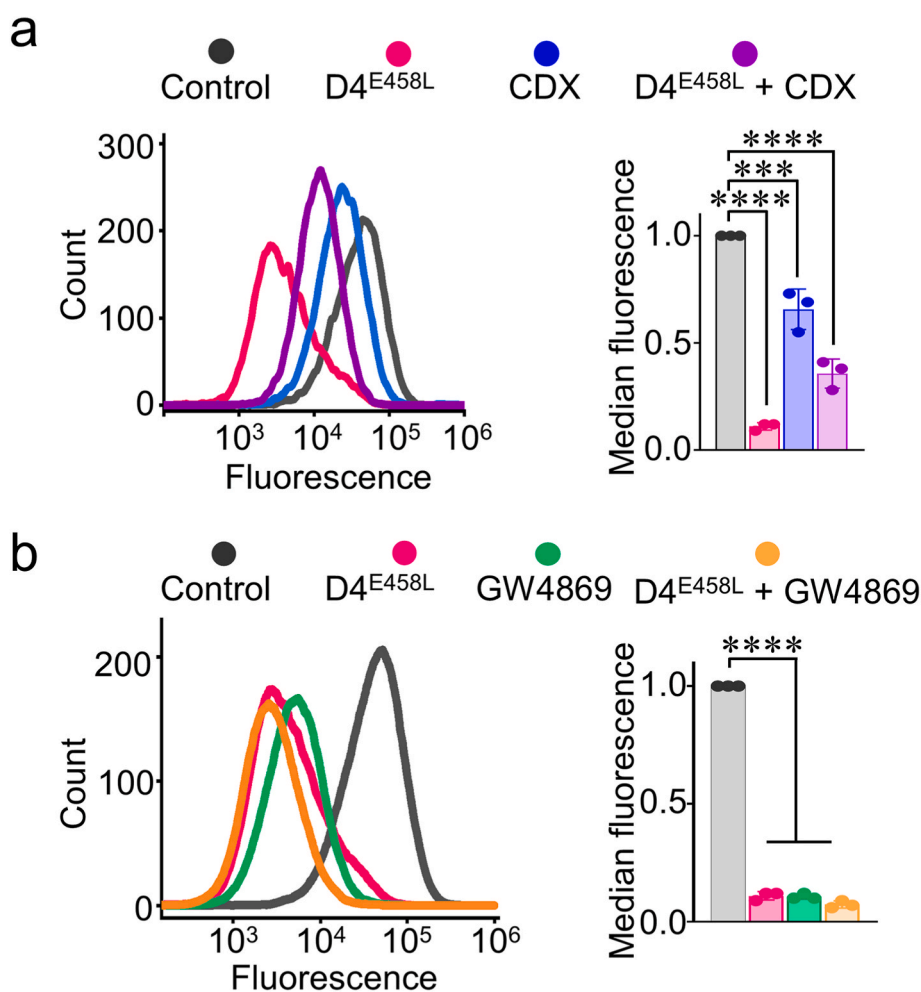


**Fig. 8.** The inhibitory effect of D4<sup>E458L</sup>, CDX and GW4869 on the internalization of Alexa-RBD in Vero E6 cells. Vero E6 cells were untreated (control) or treated with 5  $\mu$ M D4<sup>E458L</sup> and 1  $\mu$ M Alexa-RBD after pre-treatment with 5 mM CDX (a) or 5  $\mu$ M GW4869 (b). Cell fluorescence was measured by flow cytometry and is shown by representative histograms (left) and relative median fluorescence intensity (mean  $\pm$  SE) of three independent experiments (right). \*\*\*p < 0.001, \*\*\*\*p < 0.0001.

various CHOL pools in cellular processes (including membrane trafficking), their role in the uptake of viruses into the cell is not fully understood and requires further elucidation.

In the present study, we used lipid-binding proteins (nakanori and the D4 domain of PFO and its variant D4<sup>E458L</sup>) to analyze the effects of protein-membrane lipid interactions on the entry of SARS-CoV-2 into host cells. Cellular internalization of viruses depends on the plasma membrane composition and a highly regulated membrane trafficking pathways [77]. This process requires a precise balance between CHOL and sphingolipids in the plasma membrane [78,79]. Based on these considerations, we hypothesized that an effective strategy to prevent SARS-CoV-2 infection might be to target these key host plasma membrane lipids. Therapeutic doses of monoclonal antibodies suggest that lipid-binding protein concentration in the range 5–10  $\mu\text{M}$  may be realistic, with regard to efficiency and safety for therapeutic treatment. However, these types of inhibitors are not intended for systemic use, also for the reason of immunogenicity. They may be more suitable for limiting the spread of the virus on the epithelia of the respiratory tract, where less material is needed and it is easier to maintain high concentrations. On the other hand, even such concentration of protein turns out to be too high, D4 domain may act as a starting point for further development and optimization of more potent and selective molecule with improved pharmacological profile.

Our study showed that a micromolar concentration of D4 bound to the accessible CHOL in the exofacial leaflet of the plasma membrane decreases cellular uptake of fluorescently labelled virus-sized nanoparticles (Fig. 7). This suggests that the inhibitory activity of D4 on nanoparticle uptake relies on D4-induced CHOL sequestration, which hinders the membrane lipid reorganization required for membrane invagination and particle internalization. Furthermore, we showed that sequestration of membrane CHOL by micromolar concentrations of D4 also inhibits ACE2-dependent cellular internalization of fluorescently labelled RBD (Fig. 4). By contrast, binding of nakanori to SM/CHOL membrane complexes did not significantly inhibit RBD internalization at comparable concentrations, suggesting that CHOL is essential for cellular RBD uptake in specific membrane regions. Next, we demonstrated that binding of D4 and D4<sup>E458L</sup> to the plasma membrane significantly reduces virus entry into Vero E6 cells. Previously, SARS-CoV-2 entry was shown to be mediated by several pathways, including plasma membrane fusion, clathrin- and caveolae-independent or clathrin-mediated endocytic pathways [68,80–83]. Fusion of the viral envelope with the host cell plasma membrane requires proteolytic digestion of S protein by host proteases allowing release of the viral genome into the cytoplasm. Membrane fusion also occurs in the endocytic pathway when binding of ACE2 to the S protein induces virus endocytosis and fusion of the viral envelope with the endosomal membrane, allowing release of the viral genome into the cytoplasm [84,85]. However, recent studies have shown a critical role of endocytosis in SARS-CoV-2 infection of multiple cell types expressing TMPRSS2 [86]. Regardless of the route of entry, SARS-CoV-2 internalization is a lipid-raft-dependent process and requires the presence of CHOL in the plasma membrane [13,19,87]. Our results clearly show that SARS-CoV-2 entry depends on a CHOL pool in the plasma membrane, which is likely to be located in lipid rafts. We showed that sequestration of CHOL caused by D4 binding inhibits virus entry. However, the exact mechanism of action is still unclear and needs further elucidation. The sequestration of cholesterol in the plasma membrane by D4 may increase membrane tension and membrane rigidity, similarly to filipin, a commonly used sequestering agent [88], and in this way impairs virus internalization.

Our results demonstrate that D4 and its variant D4<sup>E458L</sup> reduce SARS-CoV-2 virus proliferation in Vero E6 cells and pseudovirus infection of ACE2-expressing HEK293T cells, whereas nakanori has a less potent inhibitory effect on pseudovirus or virus infection under the same experimental conditions (Figs. 5 and 6). This is probably due to the fact that nakanori binds to a different fraction of the plasma membrane than D4, which is not required for virus internalization. Indeed, biochemical

partitioning of Vero E6 cell membranes revealed predominant nakanori localization in the TX-soluble fraction, whereas D4 is co-localized with flotillin-2 in the DRM fraction (Fig. 3). Additionally, D4 binding did not change the location of the ACE2 receptor (Fig. 3), associated with the CHOL-enriched DRM fraction, which is consistent with previous reports [31,32]. Taken together, our results indicate that sequestration of CHOL, caused by the interaction of D4 with the plasma membrane, critically affects virus entry. This is similar to the effect of CDX-induced CHOL depletion from the plasma membrane of Vero E6 cells, which significantly inhibits virus production, as reported previously [10]. Similarly, the inhibitory effect of D4 is in the same range as the inhibitory effect of the commonly used pharmacological agent GW4869 (Fig. 8b), which is known to block ceramide-mediated inward budding of multivesicular bodies [89].

Interestingly, we did not observe any translocation of ACE2 from DRM to TX-soluble fraction of Vero E6 cells upon CDX treatment, even though previous studies showed such translocation of ACE2 after CHOL depletion from the plasma membrane [31]. Moreover, treatment of the plasma membrane with SMase did not alter the binding of D4 but significantly decreased binding of nakanori, indicating that the two proteins recognize different pools of SM in the plasma membrane (Fig. 3). Conversely, nakanori-mediated sequestration of CHOL from SM/CHOL complexes only slightly affected virus uptake. This suggests that the SM/CHOL complexes recognized by nakanori are not critical for virus internalization. On the other hand, it could be suggested that the composition and organization of lipids in the TX-soluble fraction of the plasma membrane hinder sequestration of CHOL by nakanori, thereby reduce its ability to inhibit virus uptake.

Our results indicate that blocking the accessibility of CHOL by binding peripheral small proteins to the plasma membrane may be an effective therapeutic strategy to treat viral infections. Binding of small lipid-binding proteins to CHOL-enriched domains of the host plasma membrane may be a useful strategy to affect the viral life cycle and prevent side effects when used in nasal applications together with other drugs [90,91]. Moreover, CHOL-enriched domains contain several molecules directly involved in SARS-CoV-2 infection (e.g., the ACE2 receptor and TMPRSS2 protease) and the immune response (e.g., Toll-like, B- and T-cell, and Fc receptors) [92]. Thus, lipid-targeting therapeutic approaches may mitigate SARS-CoV-2 infection as well as COVID-19 co-morbidities [92]. Indeed, dysregulated inflammatory processes in COVID-19 lead to abnormal immune responses that manifest in severe inflammation, cytokine storms, and sepsis [93,94]. Furthermore, long-term inflammation causes various chronic co-morbidities, such as coagulopathy or diabetes [95,96]. Therefore, influencing the abundance and accessibility of lipid components and inducing structural modifications of the plasma membrane of host cells might affect immune responses and reduce inflammation, thereby resulting in better prognosis. Furthermore, it has been suggested that cholesterol sequestration by nystatin may induce host antimicrobial defense responses by upregulation of cytokine production in macrophages, recruiting immune cells, and promoting secretion of chemokines [97]. Based on this, we can speculate that other cholesterol sequestering agents, such as the D4 domain may have an immunomodulatory effect resulting in an inhibition of viral infection.

In conclusion, our results contribute to a better understanding of the importance of the host plasma membrane CHOL in the viral life cycle. We demonstrated that specific CHOL pools in the plasma membrane of Vero E6 cells are required for SARS-CoV-2 infectivity. Moreover, our results showed that sequestration of the membrane CHOL by D4 and D4<sup>E458L</sup> inhibited entry of SARS-CoV-2 into Vero E6 cells, suggesting novel and promising therapeutic strategies against SARS-CoV-2 and possibly other viral infections. This is particularly important because the rapid viral mutagenesis and evolution associated with the development of new resistant strains represents a major challenge for the development of targeted specific antiviral vaccines and drugs. The issues associated with viral resistance could be overcome by targeting the host

plasma membrane lipids with small lipid-binding proteins.

## Funding

The work presented in this paper was supported by The Slovenian Research and Innovation Agency program grants P1-0391 and P4-0092.

## Data availability

The datasets generated during the current study are available from the corresponding author on reasonable request.

## Ethics approval

No approval of research ethics committees was required to accomplish the goals of this study because experimental work did not require any human participants, their data or biological material, or animal experiments. The virus was obtained from the European Virus Archive.

## Consent to participate

Not applicable in our case.

## Consent to publish

Not applicable in our case.

## CRediT authorship contribution statement

**Magdalena Kulma:** Conceptualization, Formal analysis, Methodology, Writing – original draft, Writing – review & editing. **Aleksandra Šakanović:** Formal analysis, Methodology, Writing – original draft, Writing – review & editing. **Apolonija Bedina-Zavec:** Formal analysis, Methodology, Writing – review & editing. **Simon Caserman:** Writing – review & editing, Methodology, Formal analysis. **Neža Omersa:** Writing – review & editing, Methodology, Formal analysis. **Gasper Solinc:** Methodology. **Sara Orehek:** Methodology. **Iva Hafner-Bratkovič:** Writing – review & editing, Methodology, Formal analysis. **Urška Kuhar:** Methodology, Formal analysis. **Brigita Slavec:** Formal analysis. **Uros Krapež:** Writing – review & editing, Methodology, Formal analysis. **Matjaž Ocepek:** Writing – review & editing, Project administration, Funding acquisition. **Toshihide Kobayashi:** Writing – review & editing. **Katarzyna Kwiatkowska:** Writing – review & editing. **Roman Jerala:** Writing – review & editing, Methodology. **Marjetka Podobnik:** Writing – review & editing, Methodology. **Gregor Anderluh:** Writing – review & editing, Writing – original draft, Supervision, Project administration, Funding acquisition, Conceptualization.

## Declaration of competing interest

The authors declare that they have no known competing financial interests or personal relationships that could have appeared to influence the work reported in this paper.

## Acknowledgments

We thank Prof. Dr. Ralf Wagner (Molecular Microbiology (Virology), Institute of Medical Microbiology and Hygiene, University of Regensburg, Germany) for pLip2\_SARS\_RBD and Prof. Dr. Stefan Pöhlmann (Infection Biology Unit, German Primate Center, Göttingen, Germany) for pCG1-SARS-2-S and pCG1-hACE2 and VSVΔG\*/G virus. We thank Patricia Tandara for laboratory work on antiviral assay experiments and Maja Jamnik and Tomaž Švigelj (Department of Molecular Biology and Nanobiotechnology, National Institute of Chemistry) for isolating and labelling RBD. We thank Dr. Eva Lasič for reviewing a draft of this manuscript.

## References

- [1] I. Koyama-Honda, T.K. Fujiwara, R.S. Kasai, et al., High-speed single-molecule imaging reveals signal transduction by induced transbilayer raft phases, *J. Cell Biol.* 219 (2020), <https://doi.org/10.1083/jcb.202006125>.
- [2] A.B. Ouweneel, M.J. Thomas, M.G. Sorci-Thomas, The ins and outs of lipid rafts: functions in intracellular cholesterol homeostasis, microparticles, and cell membranes: Thematic Review Series: biology of Lipid Rafts, *J. Lipid Res.* 61 (2020) 676–686, <https://doi.org/10.1194/jlr.TR119000383>.
- [3] S.C.D. van IJzendoorn, J. Agnetti, A. Gassama-Diagne, Mechanisms behind the polarized distribution of lipids in epithelial cells, *Biochim Biophys Acta - Biomembr.* 1862 (2020) 183145, <https://doi.org/10.1016/j.bbmem.2019.183145>.
- [4] B. Nichols, Caveosomes and endocytosis of lipid rafts, *J. Cell Sci.* 116 (2003) 4707–4714, <https://doi.org/10.1242/jcs.00840>.
- [5] H. Wei, J.-D.M. Malcor, M.T. Harper, Lipid rafts are essential for release of phosphatidylserine-exposing extracellular vesicles from platelets, *Sci. Rep.* 8 (2018) 9987, <https://doi.org/10.1038/s41598-018-28363-4>.
- [6] A. Carpinteiro, M.J. Edwards, M. Hoffmann, et al., Pharmacological inhibition of acid sphingomyelinase prevents uptake of SARS-CoV-2 by epithelial cells, *Cell reports Med* 1 (2020) 100142, <https://doi.org/10.1016/j.xcrm.2020.100142>.
- [7] I. Ripa, S. Andreu, J.A. López-Guerrero, R. Bello-Morales, Membrane rafts: portals for viral entry, *Front. Microbiol.* 12 (2021) 120.
- [8] A. Ono, E.O. Freed, Plasma membrane rafts play a critical role in HIV-1 assembly and release, *Proc Natl Acad Sci U S A* 98 (2001) 13925–13930, <https://doi.org/10.1073/pnas.241320298>.
- [9] L. Pelkmans, Secrets of caveolae- and lipid raft-mediated endocytosis revealed by mammalian viruses, *Biochim Biophys Acta - Mol Cell Res* 1746 (2005) 295–304, <https://doi.org/10.1016/j.bbamcr.2005.06.009>.
- [10] G.-M. Li, Y.-G. Li, M. Yamate, et al., Lipid rafts play an important role in the early stage of severe acute respiratory syndrome-coronavirus life cycle, *Microbes Infect* 9 (2007) 96–102, <https://doi.org/10.1016/j.micinf.2006.10.015>.
- [11] T. Takahashi, T. Suzuki, Function of membrane rafts in viral lifecycles and host cellular response, *Biochem Res Int* 2011 (2011) 245090, <https://doi.org/10.1155/2011/245090>.
- [12] X. Dou, Y. Li, J. Han, et al., Cholesterol of lipid rafts is a key determinant for entry and post-entry control of porcine rotavirus infection, *BMC Vet. Res.* 14 (2018) 45, <https://doi.org/10.1186/s12917-018-1366-7>.
- [13] R. Roncato, J. Angelini, A. Pani, R. Talotta, Lipid rafts as viral entry routes and immune platforms: a double-edged sword in SARS-CoV-2 infection? *Biochim Biophys Acta - Mol Cell Biol Lipids* 1867 (2022) 159140 <https://doi.org/10.1016/j.bbalip.2022.159140>.
- [14] Y. Lu, D.X. Liu, J.P. Tam, Lipid rafts are involved in SARS-CoV entry into Vero E6 cells, *Biochem. Biophys. Res. Commun.* 369 (2008) 344–349, <https://doi.org/10.1016/j.bbrc.2008.02.023>.
- [15] P. Bagam, D.P. Singh, M.E. Inda, S. Batra, Unraveling the role of membrane microdomains during microbial infections, *Cell Biol. Toxicol.* 33 (2017) 429–455, <https://doi.org/10.1007/s10565-017-9386-9>.
- [16] A. Makino, M. Abe, R. Ishitsuka, et al., A novel sphingomyelin/cholesterol domain-specific probe reveals the dynamics of the membrane domains during virus release and in Niemann-Pick type C, *FASEB J Off Publ Fed Am Soc Exp Biol* 31 (2017) 1301–1322, <https://doi.org/10.1096/fj.201500075R>.
- [17] M.I. Bukrinsky, N. Mukhamedova, D. Sviridov, Lipid rafts and pathogens: the art of deception and exploitation: Thematic review series: biology of lipid rafts, *J. Lipid Res.* 61 (2020) 601–610, <https://doi.org/10.1194/jlr.TR119000391>.
- [18] S. Wang, W. Li, H. Hui, et al., Cholesterol 25-Hydroxylase inhibits SARS-CoV-2 and other coronaviruses by depleting membrane cholesterol, *EMBO J.* 39 (2020) e106057, <https://doi.org/10.15252/emboj.2020106057>.
- [19] D.W. Sanders, C.C. Jumper, P.J. Ackerman, et al., SARS-CoV-2 requires cholesterol for viral entry and pathological syncytia formation, *Elife* 10 (2021) e65962, <https://doi.org/10.7554/eLife.65962>.
- [20] A. Alagheband Bahrami, A. Azarگونjahromi, S. Sadraei, et al., An overview of current drugs and prophylactic vaccines for coronavirus disease 2019 (COVID-19), *Cell. Mol. Biol. Lett.* 27 (2022) 38, <https://doi.org/10.1186/s11658-022-00339-3>.
- [21] D. Larisa, W. Adam, C. Soo-Ho, et al., Inhibition of HIV replication by apolipoprotein A-I binding protein targeting the lipid rafts, *mBio* 11 (2020) e02956, <https://doi.org/10.1128/mBio.02956-19>.
- [22] M. Glitscher, D.H. Martín, K. Woytinek, et al., Targeting cholesterol metabolism as efficient antiviral strategy against the hepatitis E virus, *Cell Mol Gastroenterol Hepatol* 12 (2021) 159–180, <https://doi.org/10.1016/j.jcmgh.2021.02.002>.
- [23] M. Glitscher, E. Hildt, Endosomal cholesterol in viral infections - a common denominator? *Front. Physiol.* 12 (2021) 750544 <https://doi.org/10.3389/fphys.2021.750544>.
- [24] S.N. Palacios-Rápalo, L.A. De Jesús-González, C.D. Cordero-Rivera, et al., Cholesterol-rich lipid rafts as platforms for SARS-CoV-2 entry, *Front. Immunol.* 12 (2021) 796855.
- [25] M. Sorice, R. Misasi, G. Riitano, et al., Targeting lipid rafts as a strategy against coronavirus, *Front. Cell Dev. Biol.* 8 (2021).
- [26] R. Lu, X. Zhao, J. Li, et al., Genomic characterisation and epidemiology of 2019 novel coronavirus: implications for virus origins and receptor binding, *Lancet* 395 (2020) 565–574, [https://doi.org/10.1016/S0140-6736\(20\)30251-8](https://doi.org/10.1016/S0140-6736(20)30251-8).
- [27] Y. Renhong, Z. Yuanyuan, L. Yaning, et al., Structural basis for the recognition of SARS-CoV-2 by full-length human ACE2, *Science* (80) 367 (2020) 1444–1448, <https://doi.org/10.1126/science.abb2762>.
- [28] H. Yang, Z. Rao, Structural biology of SARS-CoV-2 and implications for therapeutic development, *Nat. Rev. Microbiol.* 19 (2021) 685–700, <https://doi.org/10.1038/s41579-021-00630-8>.

- [29] A. Shulla, T. Heald-Sargent, G. Subramanya, et al., A transmembrane serine protease is linked to the severe acute respiratory syndrome coronavirus receptor and activates virus entry, *J. Virol.* 85 (2011) 873–882, <https://doi.org/10.1128/JVI.02062-10>.
- [30] M. Hoffmann, H. Kleine-Weber, S. Schroeder, et al., SARS-CoV-2 cell entry depends on ACE2 and TMPRSS2 and is blocked by a clinically proven protease inhibitor, *Cell* 181 (2020) 271–280.e8, <https://doi.org/10.1016/j.cell.2020.02.052>.
- [31] J. Glende, C. Schwegmann-Wessels, M. Al-Falah, et al., Importance of cholesterol-rich membrane microdomains in the interaction of the S protein of SARS-coronavirus with the cellular receptor angiotensin-converting enzyme 2, *Virology* 381 (2008) 215–221, <https://doi.org/10.1016/j.virol.2008.08.026>.
- [32] R.A. Ballout, D. Sviridov, M.I. Bukrinsky, A.T. Remaley, The lysosome: a potential juncture between SARS-CoV-2 infectivity and Niemann-Pick disease type C, with therapeutic implications, *FASEB J* 34 (2020) 7253–7264, <https://doi.org/10.1096/fj.202000654R>.
- [33] M. Dal Peraro, F.G. van der Goot, Pore-forming toxins: ancient, but never really out of fashion, *Nat. Rev. Microbiol.* 14 (2016) 77–92, <https://doi.org/10.1038/nrmicro.2015.3>.
- [34] R.K. Tweten, E.M. Hotze, K.R. Wade, The unique molecular Choreography of giant pore formation by the cholesterol-dependent cytolysins of Gram-positive bacteria, *Annu. Rev. Microbiol.* 69 (2015) 323–340, <https://doi.org/10.1146/annurev-micro-091014-104233>.
- [35] Y. Shimada, M. Maruya, S. Iwashita, Y. Ohno-Iwashita, The C-terminal domain of perfringolysin O is an essential cholesterol-binding unit targeting to cholesterol-rich microdomains, *Eur. J. Biochem.* 269 (2002) 6195–6203, <https://doi.org/10.1046/j.1432-1033.2002.03338.x>.
- [36] Y. Ohno-Iwashita, Y. Shimada, A.A. Waheed, et al., Perfringolysin O, a cholesterol-binding cytolysin, as a probe for lipid rafts, *Anaerobe* 10 (2004) 125–134, <https://doi.org/10.1016/j.anaerobe.2003.09.003>.
- [37] A. Gay, D. Rye, A. Radhakrishnan, Switch-like responses of two cholesterol sensors do not require protein oligomerization in membranes, *Biophys. J.* 108 (2015) 1459–1469, <https://doi.org/10.1016/j.bpj.2015.02.008>.
- [38] S.-L. Liu, R. Sheng, J.H. Jung, et al., Orthogonal lipid sensors identify transbilayer asymmetry of plasma membrane cholesterol, *Nat. Chem. Biol.* 13 (2017) 268–274, <https://doi.org/10.1038/nchembio.2268>.
- [39] M. Maekawa, Y. Yang, G.D. Fairn, Perfringolysin O Theta toxin as a tool to monitor the distribution and inhomogeneity of cholesterol in cellular membranes, *Toxins* 8 (2016), <https://doi.org/10.3390/toxins8030067>.
- [40] E. Lasić, M. Lisjak, A. Horvat, et al., Astrocyte specific Remodeling of plasmalemmal cholesterol composition by Ketamine indicates a new mechanism of Antidepressant action, *Sci. Rep.* 9 (2019) 10957, <https://doi.org/10.1038/s41598-019-47459-z>.
- [41] B. Rütuper, A. Guček, M. Lisjak, et al., Vesicle cholesterol controls exocytotic fusion pore, *Cell Calcium* 101 (2022) 102503, <https://doi.org/10.1016/j.ceca.2021.102503>.
- [42] A.M. Bryan, J.K. You, G. Li, et al., Cholesterol and sphingomyelin are critical for Fcγ receptor-mediated phagocytosis of <em>Cryptococcus neoformans</em> by macrophages, *J. Biol. Chem.* 297 (2021), <https://doi.org/10.1016/j.jbc.2021.101411>.
- [43] J. Lan, J. Ge, J. Yu, et al., Structure of the SARS-CoV-2 spike receptor-binding domain bound to the ACE2 receptor, *Nature* 581 (2020) 215–220, <https://doi.org/10.1038/s41586-020-2180-5>.
- [44] J.F. Dishinger, H.L. Kee, K.J. Verhey, Chapter five - analysis of Ciliary Import, in: W.F.B.T.-M. Marshall (Ed.), *Cilia, Part A*, Academic Press, 2013, pp. 75–89.
- [45] K. Kwiatkowska, E. Marszałek-Sadowska, G. Traczyk, et al., Visualization of cholesterol deposits in lysosomes of Niemann-Pick type C fibroblasts using recombinant perfringolysin O, *Orphanet J. Rare Dis.* 9 (2014) 64, <https://doi.org/10.1186/1750-1172-9-64>.
- [46] A. Bavdek, N.O. Gekara, D. Priselac, et al., Sterol and pH interdependence in the binding, oligomerization, and pore formation of Listeriolysin O, *Biochemistry* 46 (2007) 4425–4437, <https://doi.org/10.1021/bi602497g>.
- [47] G. Anderlüh, M. Besenicar, A. Kladnik, et al., Properties of nonfused lysosomes immobilized on an L1 Biacore chip and their permeabilization by a eukaryotic pore-forming toxin, *Anal. Biochem.* 344 (2005) 43–52, <https://doi.org/10.1016/j.ab.2005.06.013>.
- [48] A. Šakanović, V. Hodnik, G. Anderlüh, in: J.H. Kleinschmidt (Ed.), *Surface Plasmon Resonance for Measuring Interactions of Proteins with Lipids and Lipid Membranes BT - Lipid-Protein Interactions: Methods and Protocols*, Springer, New York, New York, NY, 2019, pp. 53–70.
- [49] M. Berger Rentsch, G. Zimmer, A vesicular stomatitis virus Replicon-based bioassay for the rapid and sensitive determination of multi-species type I interferon, *PLoS One* 6 (2011) e25858.
- [50] M. Manček-Keber, I. Hafner-Bratkovič, D. Lainšček, et al., Disruption of disulfides within RBD of SARS-CoV-2 spike protein prevents fusion and represents a target for viral entry inhibition by registered drugs, *FASEB J* 35 (2021) e21651, <https://doi.org/10.1096/fj.202100560R>.
- [51] D. Lainšček, T. Fink, V. Forstnerič, et al., A Nanoscaffolded spike-RBD vaccine Protection against SARS-CoV-2 with Minimal anti-Scaffold response, *Vaccines* 9 (2021), <https://doi.org/10.3390/vaccines9050431>.
- [52] V.M. Corman, O. Landt, M. Kaiser, et al., Detection of 2019 novel coronavirus (2019-nCoV) by real-time RT-PCR, *Euro Surveill.* 25 (2020), <https://doi.org/10.2807/1560-7917.ES.2020.25.3.2000045>.
- [53] G. Riedel, U. Rüdlich, N. Fekete-Drimusz, et al., An extended ΔCT-method facilitating normalisation with multiple reference genes suited for quantitative RT-PCR analyses of human Hepatocyte-like cells, *PLoS One* 9 (2014) e93031.
- [54] A. Šakanović, N. Kranjc, N. Omersa, et al., More than one way to bind to cholesterol: atypical variants of membrane-binding domain of perfringolysin O selected by ribosome display, *RSC Adv.* 10 (2020) 38678–38682, <https://doi.org/10.1039/D0RA06976K>.
- [55] G. Anderlüh, I. Gökçe, J.H. Lakey, Expression of proteins using the third domain of the Escherichia coli periplasmic-protein TolA as a fusion partner, *Protein Expr. Purif.* 28 (2003) 173–181, [https://doi.org/10.1016/S1046-5928\(02\)00681-2](https://doi.org/10.1016/S1046-5928(02)00681-2).
- [56] M. Maekawa, Domain 4 (D4) of perfringolysin O to visualize cholesterol in cellular membranes-the Update, *Sensors* 17 (2017) 504, <https://doi.org/10.3390/s17030504>.
- [57] E. London, D.A. Brown, Insolubility of lipids in Triton X-100: physical origin and relationship to sphingolipid/cholesterol membrane domains (rafts), *Biochim Biophys Acta - Biomembr* 1508 (2000) 182–195, [https://doi.org/10.1016/S0304-4157\(00\)00007-1](https://doi.org/10.1016/S0304-4157(00)00007-1).
- [58] A.A. Waheed, Y. Shimada, H.F.G. Heijnen, et al., Selective binding of perfringolysin O derivative to cholesterol-rich membrane microdomains (rafts), *Proc Natl Acad Sci* 98 (2001), <https://doi.org/10.1073/pnas.091090798>, 4926 LP – 4931.
- [59] A.C. Walls, Y.-J. Park, M.A. Tortorici, et al., Structure, function, and Antigenicity of the SARS-CoV-2 spike glycoprotein, *Cell* 181 (2020) 281–292.e6, <https://doi.org/10.1016/j.cell.2020.02.058>.
- [60] X. Tian, C. Li, A. Huang, et al., Potent binding of 2019 novel coronavirus spike protein by a SARS coronavirus-specific human monoclonal antibody, *Emerg. Microbes Infect.* 9 (2020) 382–385.
- [61] C. Forest-Nault, I. Koyuturk, J. Gaudreault, et al., Impact of the temperature on the interactions between common variants of the SARS-CoV-2 receptor binding domain and the human ACE2, *Sci. Rep.* 12 (2022) 11520, <https://doi.org/10.1038/s41598-022-15215-5>.
- [62] D. Raghu, P. Hamill, A. Banaji, et al., Assessment of the binding interactions of SARS-CoV-2 spike glycoprotein variants, *J Pharm Anal* 12 (2022) 58–64, <https://doi.org/10.1016/j.jpfa.2021.09.006>.
- [63] S. Mazumdar, D. Chitkara, A. Mittal, Exploration and insights into the cellular internalization and intracellular fate of amphiphilic polymeric nanocarriers, *Acta Pharm. Sin. B* 11 (2021) 903–924, <https://doi.org/10.1016/j.apsb.2021.02.019>.
- [64] S. Behzadi, V. Serpooshan, W. Tao, et al., Cellular uptake of nanoparticles: journey inside the cell, *Chem. Soc. Rev.* 46 (2017) 4218–4244, <https://doi.org/10.1039/C6CS00636A>.
- [65] M. Maekawa, G.D. Fairn, Complementary probes reveal that phosphatidylserine is required for the proper transbilayer distribution of cholesterol, *J. Cell Sci.* 128 (2015) 1422–1433, <https://doi.org/10.1242/jcs.164715>.
- [66] M. Maekawa, M. Lee, K. Wei, et al., Staurosporines decrease ORMDL proteins and enhance sphingomyelin synthesis resulting in depletion of plasmalemmal phosphatidylserine, *Sci. Rep.* 6 (2016) 35762, <https://doi.org/10.1038/srep35762>.
- [67] R. Ishitsuka, T. Saito, H. Osada, et al., Fluorescence image screening for chemical compounds modifying cholesterol metabolism and distribution[S], *J. Lipid Res.* 52 (2011) 2084–2094, <https://doi.org/10.1194/jlr.D018184>.
- [68] H. Wang, P. Yang, K. Liu, et al., SARS coronavirus entry into host cells through a novel clathrin- and caveolae-independent endocytic pathway, *Cell Res.* 18 (2008) 290–301, <https://doi.org/10.1038/cr.2008.15>.
- [69] J. Kornhuber, N. Hoertel, E. Gulbins, The acid sphingomyelinase/ceramide system in COVID-19, *Mol Psychiatry* 27 (2022) 307–314, <https://doi.org/10.1038/s41380-021-01309-5>.
- [70] C. Mühle, A. Kremer, M. Vetter, et al., COVID-19 and its clinical severity are associated with alterations of plasma sphingolipids and enzyme activities of sphingomyelinase and ceramidase, *medRxiv* (2022), <https://doi.org/10.1101/2022.01.19.22269391>, 2022.01.19.22269391.
- [71] E.H. Alkhetib, R. Hamdy, A. El-Kabalawy, et al., Lipid-based therapies against SARS-CoV-2 infection, *Rev. Med. Virol.* 31 (2021) e2214, <https://doi.org/10.1002/rmv.2214>.
- [72] R. Nardacci, F. Colavita, C. Castilletti, et al., Evidences for lipid involvement in SARS-CoV-2 cytopathogenesis, *Cell Death Dis.* 12 (2021) 263, <https://doi.org/10.1038/s41419-021-03527-9>.
- [73] S. Surma, M. Banach, J. Lewek, COVID-19 and lipids. The role of lipid disorders and statin use in the prognosis of patients with SARS-CoV-2 infection, *Lipids Health Dis.* 20 (2021) 141, <https://doi.org/10.1186/s12944-021-01563-0>.
- [74] A. Das, M.S. Brown, D.D. Anderson, et al., Three pools of plasma membrane cholesterol and their relation to cholesterol homeostasis, *Elife* 3 (2014), <https://doi.org/10.7554/eLife.02882>.
- [75] R.E. Infante, A. Radhakrishnan, Continuous transport of a small fraction of plasma membrane cholesterol to endoplasmic reticulum regulates total cellular cholesterol, *Elife* 6 (2017) e25466, <https://doi.org/10.7554/eLife.25466>.
- [76] K.A. Johnson, S. Endapally, D.C. Vazquez, et al., Ostreolysin A and anthrolysin O use different mechanisms to control movement of cholesterol from the plasma membrane to the endoplasmic reticulum, *J. Biol. Chem.* 294 (2019) 17289–17300, <https://doi.org/10.1074/jbc.RA119.010393>.
- [77] M. Robinson, S. Schor, R. Barouch-Bentov, S. Einav, Viral journeys on the intracellular highways, *Cell. Mol. Life Sci.* 75 (2018) 3693–3714, <https://doi.org/10.1007/s00018-018-2882-0>.
- [78] H. Pichler, H. Riezman, Where sterols are required for endocytosis, *Biochim. Biophys. Acta* 1666 (2004) 51–61, <https://doi.org/10.1016/j.bbmem.2004.05.011>.
- [79] J.T. Hannich, K. Umebayashi, H. Riezman, Distribution and functions of sterols and sphingolipids, *Cold Spring Harb Perspect Biol* 3 (2011) a004762, <https://doi.org/10.1101/cshperspect.a004762>.

- [80] S. Wang, F. Guo, K. Liu, et al., Endocytosis of the receptor-binding domain of SARS-CoV spike protein together with virus receptor ACE2, *Virus Res.* 136 (2008) 8–15, <https://doi.org/10.1016/j.virusres.2008.03.004>.
- [81] K. Gorshkov, K. Susumu, J. Chen, et al., Quantum dot-conjugated SARS-CoV-2 spike Pseudo-Virions enable tracking of angiotensin converting enzyme 2 binding and endocytosis, *ACS Nano* 14 (2020) 12234–12247, <https://doi.org/10.1021/acsnano.0c05975>.
- [82] A. Bayati, R. Kumar, V. Francis, P.S. McPherson, SARS-CoV-2 infects cells after viral entry via clathrin-mediated endocytosis, *J. Biol. Chem.* 296 (2021) 100306, <https://doi.org/10.1016/j.jbc.2021.100306>.
- [83] C. Prabhakara, R. Godbole, P. Sil, et al., Strategies to target SARS-CoV-2 entry and infection using dual mechanisms of inhibition by acidification inhibitors, *PLoS Pathog.* 17 (2021) e1009706.
- [84] R. Peng, L.-A. Wu, Q. Wang, et al., Cell entry by SARS-CoV-2, *Trends Biochem. Sci.* 46 (2021) 848–860, <https://doi.org/10.1016/j.tibs.2021.06.001>.
- [85] C.B. Jackson, M. Farzan, B. Chen, H. Choe, Mechanisms of SARS-CoV-2 entry into cells, *Nat. Rev. Mol. Cell Biol.* 23 (2022) 3–20, <https://doi.org/10.1038/s41580-021-00418-x>.
- [86] A.J.B. Kreutzberger, A. Sanyal, A. Saminathan, et al., SARS-CoV-2 requires acidic pH to infect cells, *Proc Natl Acad Sci* 119 (2022) e2209514119, <https://doi.org/10.1073/pnas.2209514119>.
- [87] T. Tang, M. Bidon, J.A. Jaimes, et al., Coronavirus membrane fusion mechanism offers a potential target for antiviral development, *Antiviral Res* 178 (2020) 104792, <https://doi.org/10.1016/j.antiviral.2020.104792>.
- [88] L. Bonneau, P. Gerbeau-Pissot, D. Thomas, et al., Plasma membrane sterol complexation, generated by filipin, triggers signaling responses in tobacco cells, *Biochim. Biophys. Acta* 1798 (2010) 2150–2159, <https://doi.org/10.1016/j.bbmem.2010.07.026>.
- [89] K. Menck, C. Sönmezer, T.S. Worst, et al., Neutral sphingomyelinases control extracellular vesicles budding from the plasma membrane, *J. Extracell. Vesicles* 6 (2017) 1378056, <https://doi.org/10.1080/20013078.2017.1378056>.
- [90] N.A. Ratcliffe, H.C. Castro, I.C. Paixão, et al., Nasal therapy—the missing link in optimising strategies to improve prevention and treatment of COVID-19, *PLoS Pathog.* 17 (2021) e1010079.
- [91] T. Shapira, I.A. Monreal, S.P. Dion, et al., A TMPRSS2 inhibitor acts as a pan-SARS-CoV-2 prophylactic and therapeutic, *Nature* 605 (2022) 340–348, <https://doi.org/10.1038/s41586-022-04661-w>.
- [92] P. Varshney, V. Yadav, N. Saini, Lipid rafts in immune signalling: current progress and future perspective, *Immunology* 149 (2016) 13–24, <https://doi.org/10.1111/imm.12617>.
- [93] H. Li, L. Liu, D. Zhang, et al., SARS-CoV-2 and viral sepsis: observations and hypotheses, *Lancet (London, England)* 395 (2020) 1517–1520, [https://doi.org/10.1016/S0140-6736\(20\)30920-X](https://doi.org/10.1016/S0140-6736(20)30920-X).
- [94] B. Hu, S. Huang, L. Yin, The cytokine storm and COVID-19, *J. Med. Virol.* 93 (2021) 250–256, <https://doi.org/10.1002/jmv.26232>.
- [95] W. Miesbach, M. Makris, COVID-19: coagulopathy, risk of Thrombosis, and the rationale for anticoagulation, *Clin Appl Thromb Off J Int Acad Clin Appl Thromb* 26 (2020) 1076029620938149, <https://doi.org/10.1177/1076029620938149>.
- [96] S.E. Daugherty, Y. Guo, K. Heath, et al., Risk of clinical sequelae after the acute phase of SARS-CoV-2 infection: retrospective cohort study, *BMJ* 373 (2021) n1098, <https://doi.org/10.1136/bmj.n1098>.
- [97] X. Zhang, T. Li, X. Chen, et al., Nystatin enhances the immune response against *Candida albicans* and protects the ultrastructure of the vaginal epithelium in a rat model of vulvovaginal candidiasis, *BMC Microbiol.* 18 (2018) 166, <https://doi.org/10.1186/s12866-018-1316-3>.